Summer June, 2018

Jänecke et al. 2018 Durmid SAF Lithosphere.pdf

Susanne U. Jänecke, *Utah State University*
Daniel K. Markowski

THE GEOLOGICAL SOCIETY OF AMERICA®

Durmid ladder structure and its implications for the nucleation sites of the next M >7.5 earthquake on the San Andreas fault or Brawley seismic zone in southern California

Susanne U. Jänecke[1], Daniel K. Markowski[1,*], James P. Evans[1], Patricia Persaud[2], and Miles Kenney[3]
[1]DEPARTMENT OF GEOLOGY, UTAH STATE UNIVERSITY, 4505 OLD MAIN HILL, LOGAN, UTAH 84322-4505, USA
[2]DEPARTMENT OF GEOLOGY AND GEOPHYSICS, LOUISIANA STATE UNIVERSITY, E235 HOWE-RUSSELL-KNIFFEN, BATON ROUGE, LOUISIANA 70803, USA
[3]KENNEY GEOSCIENCE, OCEANSIDE, CALIFORNIA 92058, USA

ABSTRACT

We integrated new geologic data with published geophysical data to document that the southernmost San Andreas fault zone, onshore of the Salton Sea, southern California, is a transpressional, 1–4-km-wide ladder-like structure. This newly identified Durmid ladder structure is a voluminous right-reverse fault zone that broadens across Durmid Hill around rotating domains of regularly spaced, left- and right-lateral cross faults. The active East Shoreline fault zone of the San Andreas fault forms the southwest margin of this fault zone, and it is generally parallel to the main strand of the San Andreas fault zone for >30 km, deforms Pliocene to modern sediment, and has an ~1-km-wide damage zone of strongly folded and faulted sedimentary rocks. Hundreds of left- and right-lateral cross faults and folds connect the two right-lateral strands of the San Andreas fault zone within the ladder structure for at least 25 km northward from Bombay Beach. Left-lateral cross faults strike east and likely rotated clockwise ~45°–60° from their original northeast strike. Transpression, clockwise rotation, and right-lateral shear between the East Shoreline fault and main strand of the San Andreas fault zone in the Durmid ladder structure exhumed a large amount of Pliocene–Pleistocene basin fill since the ladder formed in the Pleistocene.

Strike-slip faults in the Durmid ladder structure cut latest Cenozoic to modern sediment and produced many of the ubiquitous folds in the area by fault-bend folding as they slipped past ramps and flats. Growth strata in the upper Brawley Formation are concentrated along the master right-lateral fault zones. Long, narrow zones of fractures displace modern sediment along both edges of the Durmid structure, perhaps due to the same kind of slow shallow creep that has been documented along the main strand of the San Andreas fault zone. Steep right and right-oblique faults and folds are the main structures in Pleistocene sediments deformed by the ~1-km-wide East Shoreline fault. Geophysical data sets and drill holes in Coachella Valley show that the East Shoreline fault probably persists into the subsurface as a northeast-dipping fault zone that defines the basinward edge of a complex three-dimensional flower structure along ~100 km of the San Andreas fault zone.

The East Shoreline fault appears to continue northward for over 100 km past the Mecca and Indio Hills along the northeast margin of Coachella Valley, where southwest-dipping basin-fill deposits are being exhumed on its northeast side. Lines 4 and 5 of the Salton Seismic Imaging Project imaged faults that are along strike of the East Shoreline fault and occupy the same structural position as the East Shoreline fault relative to the San Andreas fault. These data are also consistent with the East Shoreline fault being related to the Garnet Hills fault of the San Andreas fault zone. Southward, the transpressional southernmost San Andreas fault zone changes gradually along strike into the transtensional Brawley seismic zone across an ~5-km-long transitional zone. Several-kilometer-wide strike-slip fault zones, like those documented here, occur along many active faults, including some in metropolitan areas. Their implications for ground-shaking and surface faulting hazards are currently overlooked, and they are not considered in California's Alquist-Priolo Earthquake Fault Zones.

LITHOSPHERE https://doi.org/10.1130/L629.1

BACKGROUND AND MOTIVATION

Geoscientists are watchful of any changes along the Coachella Valley section of the San Andreas fault zone (SAFZ). The last major earthquake on the SAFZ here occurred ca. 1690 CE (Philibosian et al., 2011). The average recurrence interval along this section is 116–221 yr, making it twice as likely to rupture as most of the other faults in California (Philibosian et al., 2011; Field et al., 2014, 2015). The southern tip of the fault might also be the nucleation point of a future M ≥ 7.5 earthquake on the San Andreas fault because this site is interpreted as an interaction zone between left-lateral or left-oblique faults under the Salton Sea and the SAFZ (Hudnut et al., 1989a, 1989b; Olsen et al., 1995, 2006, 2009; Jones et al., 2008; Brothers et al., 2009, 2011; Field et al., 2014, 2015; Jordan, 2016).

*Present address: Shannon and Wilson, Inc., 1321 Bannock St., #200, Denver, Colorado 80204, USA.

Despite its significance, large uncertainties remain regarding the fundamental structural geometry of the SAFZ along its southern 15–30-km-long trace, the interactions between the SAFZ and active faults on either side, interactions along strike, the transpressional or transtensional component of deformation near the Salton Sea, and the distribution and importance of creep and triggered slip along this trace (Babcock, 1974; Clark, 1984; Bürgmann, 1991; Hudnut et al., 1989a, 1989b; Brothers et al., 2011; Tong et al., 2013; Lindsey et al., 2014). These uncertainties, the model earthquake scenario used in the ShakeOut earthquake preparedness exercise in southern California (Jones et al., 2008; Olsen et al., 2009), and the prediction of extensional deformation (Hudnut et al., 1989a, 1989b; Brothers et al., 2011), where only shortening and strike-slip motion are known, motivated our new analyses at the southern tip of the fault zone.

The Coachella Valley segment of the SAFZ extends from the southwest edge of Indio Hills southeastward toward Bombay Beach near the shallow northeastern margin of the Salton Sea (Fig. 1). The seismically quiet SAFZ gives way to the seismically active Brawley seismic zone (BSZ) ~1.5 km east of Bombay Beach under the shallowest edge of the Salton Sea (Figs. 1 and 2; Lin et al., 2007; Hauksson et al., 2012; Lin, 2013). The SAFZ is well exposed along Durmid Hill, the area between

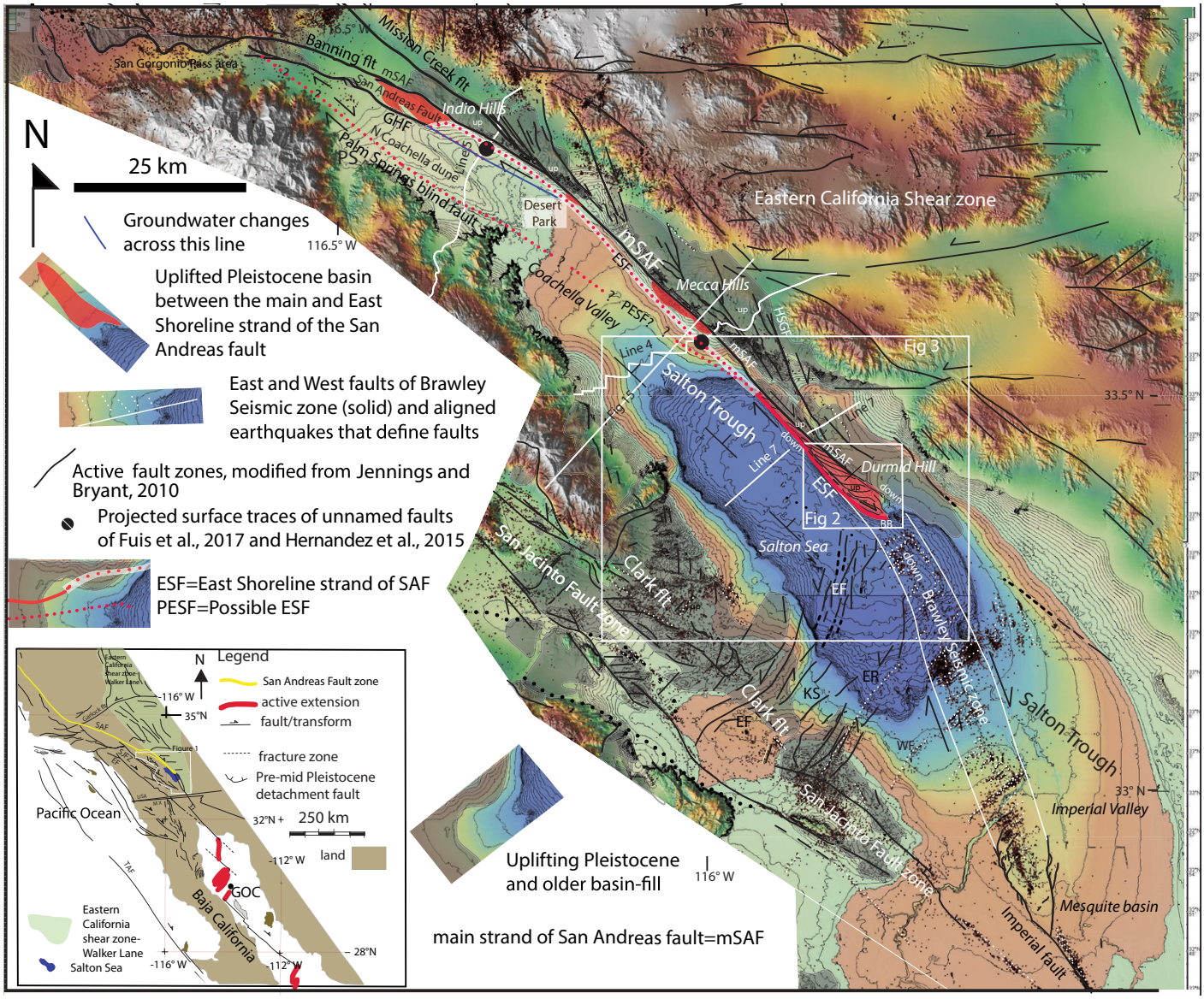

Figure 1. Map showing the faults and uplifting late Cenozoic basin fill (gray) of southeastern California. Relocated earthquakes (dark brown) from Hauksson et al. (2012) illuminate the map view locations of faults with seismicity since 1981. We show here that the East Shoreline fault zone (ESF) continues north along the northeast margin of the Salton Trough, where it defines the southwest edge of uplifted basin fill in the western Mecca Hills and at Desert Park farther north (red shading). Lines 4 and 5 of the Salton Seismic Imaging Project documented northeast-dipping reflections from the several fault zones around the black dots (Fuis et al., 2017; Hernandez et al., 2015). The ESF might also cross Coachella Valley to join the blind Palm Spring right-reverse fault (Janecke and Markowski, 2013), and this speculative trace is labelled as PESF. The northwest end of the blind Palm Spring fault is fault F3 of Carena et al. (2004), and it dips 70° toward N35°E, where it produced earthquakes. mSAF—main strand of the San Andreas fault; BB—Bombaby Beach; GHF—Garnet Hills fault; GOC—Gulf of California; EF—Extra fault array; EF (inset)—Elsinore fault zone; ER—Elmore Ranch fault array; HSGF—Hidden Springs–Grotto fault zone; PS—Palm Springs; WF—Westmoreland swarm fault; KS—Kane Springs fault; flt—fault; SJFZ—San Jacinto fault zone; TAF—Tosco-Abriejos fault.

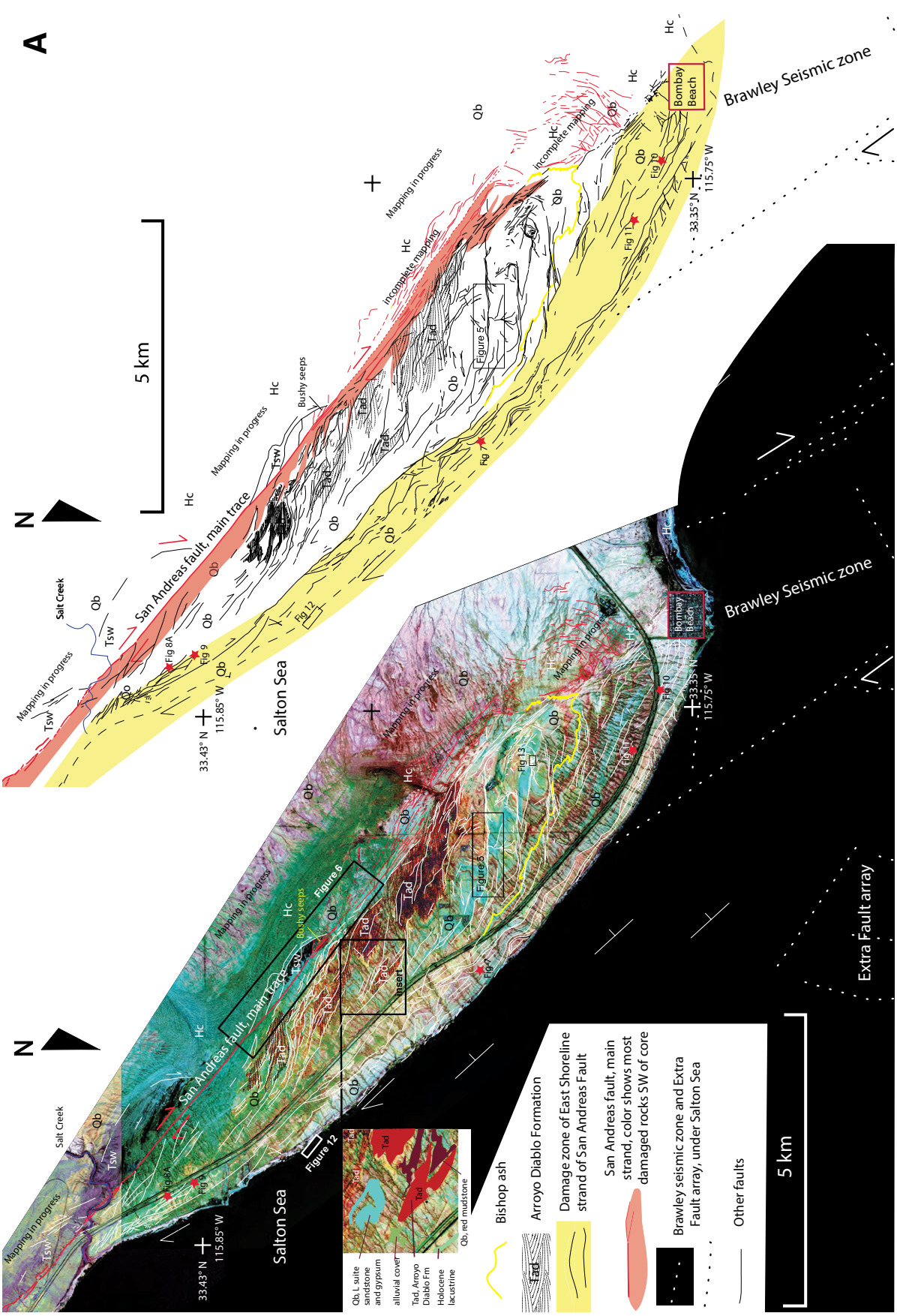

Figure 2. (A) Geologic and fault map of the San Andreas fault zone (SAFZ) in Durmid Hill plotted on a false-color National Agriculture Imagery Program (NAIP) digital aerial image processed to highlight different compositions of the sedimentary rocks and sediment (see insert). The map on the right shows the damage zones along the main strand and East Shoreline strands of the SAFZ, in red and yellow shading, respectively. We exclude the much less deformed rock in the damage zone on the northeast side of the mSAF from this shading. The mSAF is a thick red line where it is a simple fault zone and thin where it branches. Submerged traces of faults of the Brawley Seismic zone (BSZ) and Extra fault array are traced or interpreted from the data of Shearer et al. (2005), Brothers (2009), Lin (2013), Hauksson et al. (2012), and Hauksson (2016, written comm.). See Markowski (2016) for a complete geologic map that includes the marker units shown in Fig. 4. Hc—Holocene sediment, dominantly of Lake Cahuilla; Qb—Brawley Formation; Tad—Arroyo Diablo Formation; Tsw—Shavers Well Formation. Southeast of the bushy seeps (BS), the mSAF has many diverging traces. Rectangular outlines show the locations of Figures 5, 6, 12, and 13, and the explanation of formations. Stars designate the location of outcrops in Figures 7–11. (*Continued on following page.*)

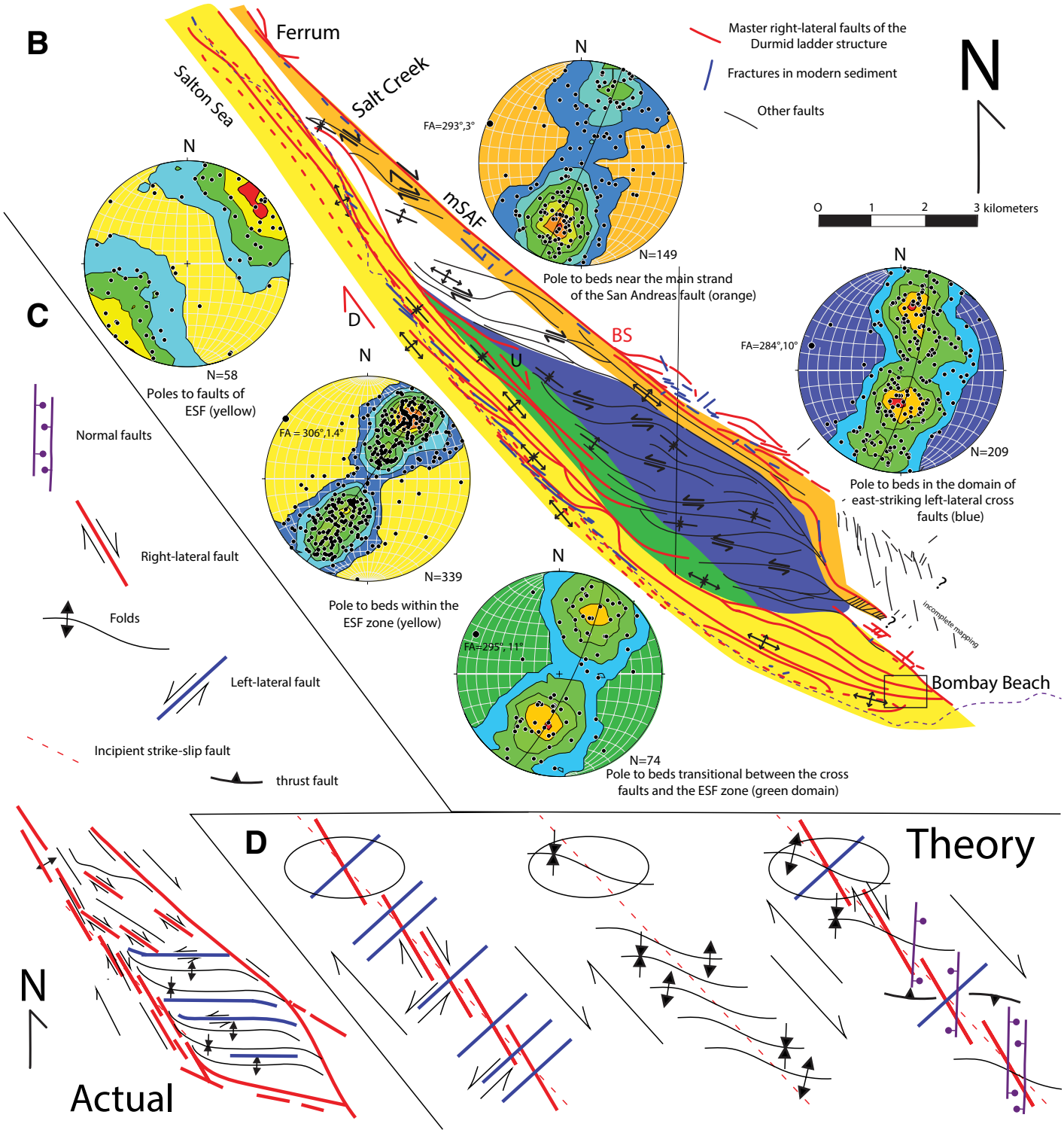

Figure 2 (*continued*). (B) Color-coded stereograms are equal-area Kamb contours of bedding in each of four structural domains shown in the index map. A fifth plot shows that faults within the ESF zone strike northwest and range in their dip values and dip direction. Southeast of the bushy seeps (BS), the mSAF has many diverging traces. Fractures in modern sediment are dark blue. FA—cylindrical best-fit fold axis. (C) Simplified sketch of faults and folds in part of the Durmid ladder structure. (D) Expected geometries of strike-slip related structures in map view according to kinematic models of Sylvester (1988). These geometries depict the initial stages of deformation in the stress field of southern California. The actual strikes of the rotated left-lateral faults in the cross-fault domain of Durmid Hill (A, B, and C) and the similar trends of folds and strike-slip faults there disagree with the expected geometries.

Salt Creek and Bombay Beach (Figs. 1 and 2), and this part of the plate boundary has been the focus of several studies (Dibblee, 1954, 1997; Babcock, 1969, 1974; Bilham and Williams, 1985; Lindvall et al., 1989; Sieh and Williams, 1990; Bürgmann, 1991; Hudnut et al., 1989a, 1989b; Sylvester et al., 1993; Dibblee and Minch, 2008a, 2008b, 2008c; Brothers et al., 2011; Fuis et al., 2012, 2017; Lindsey and Fialko, 2013; Lindsey et al., 2014). Durmid Hill is a local highpoint on an elongated ridge that parallels the main strand of the San Andreas fault (hereafter referred to as mSAF) on its northeast side (Figs. 1, 2, and 3). The fault zone and the rocks southwest of the mSAF consist of highly deformed Pliocene–Pleistocene deposits (Babcock, 1974; Bürgmann, 1991; Markowski, 2016). The same formations are much less deformed northeast of the mSAF zone (Fig. 2; Babcock, 1974; Markowski, 2016).

Determining the geometry of the southern 15 km of the SAFZ is challenging due to the presence of very faulted and folded rocks and sediments, patchy exposure, the presence of similar lithofacies that repeat in the Pliocene–Holocene sedimentary rocks (Fig. 4), the subtle expressions of some faults in the landscape, and the variable and quasi–en echelon geometries of the faults and folds in the area. Lake Cahuilla has repeatedly inundated the Salton Trough during the last ~1420 yr (ages from Rockwell, 2016), and the 1905–1907 flooding by the Colorado River eroded or covered many of the geomorphic features that normally highlight active faults. Waves in these modern and latest Holocene lakes carved a gently sloping surface on the western edge of Durmid Hill and built some beach ridges and spits across its crest. The most extensive lacustrine deposits and wave-cut shorelines are within 10–15 m of the highest shorelines. Durmid Hill was completely submerged beneath Lake Cahuilla several times during the last thousand years (Rockwell, 2016), except near Bat Caves Butte. Rapid desiccation at the end of each lake cycle, and the associated drop in base level led to the incision of hundreds of 1–4-m-deep gullies on the southwest flank of Durmid Hill. Due to these challenges, many key relationships and most of the faults of Durmid Hill were first identified by Markowski (2016) and this study.

Previous workers speculated on, and disagreed about, the location of the mSAF between the crest of Durmid Hill and the Salton Sea through the patchy exposure along the southern 4–7 km of the fault zone (Figs. 1, 2, and 3; Dibblee, 1954, 1997; Babcock, 1969, 1974; Clark, 1984; Bilham and Williams, 1985; Bürgmann, 1991; Jennings, 1967, 1994; Hope, 1969; Dibblee and Minch, 2008a, 2008b, 2008c; Lynch and Hudnut, 2008; Brothers et al., 2009, 2011; Bryant, 2015). Two competing interpretations emerged. One interpretation envisions a southeastward continuation of the mSAF with a consistent strike that projects toward the Sand Dune fault zone along the margin of the Salton Trough (Babcock, 1974; Jennings, 1967, 1994), whereas the second interpretation holds that the San Andreas fault curves southward, and bends to a more northerly strike ~5 km northwest of Bombay Beach, California. Neither option is well documented, yet most fault maps currently depict the active trace of the southernmost SAFZ as bending.

Southwest of the mSAF, the Extra fault zone was first recognized near the San Jacinto fault zone as a sequence of left-lateral strike-slip faults that strike northeast, at a high angle to the SAFZ (EF in Fig. 1; Dibblee, 1954; Hudnut et al.,1989a, 1989b). Subsequent study showed the Extra fault to be the central left-lateral fault of an 8–10-km-wide fault array that resembles the Elmore Ranch fault array of the Superstition Hills, and that it persists into the Salton Sea after bending to a north-northeasterly strike (Hudnut et al., 1989a, 1989b; Brothers et al., 2009, 2011; Thornock, 2013). Seismic rupture models for the southern tip of the SAFZ envision secondary effects of left-lateral or left-normal earthquakes in the Extra fault array as modulating stress or unclamping the SAFZ in the southern part of Durmid Hill enough to trigger a large northward-propagating rupture along the mSAF (Hudnut et al., 1989a, 1989b; Brothers et al., 2011). Previous geologic mapping and structural analysis documented the highly shortened nature of the Pliocene to Pleistocene sedimentary rocks in the Durmid Hill area on the southwest side of the SAFZ, however, and did not show any structural evidence for the extension or left-lateral stress modulation by structures related to the Extra fault array that are predicted by the cross-fault models (Dibblee, 1954, 1997; Babcock, 1969, 1974; Bürgmann, 1991; Dibblee and Minch, 2008a, 2008b, 2008c). Instead, prior field studies documented extensively folded Pleistocene deposits southwest of the SAFZ in Durmid Hill.

Bürgmann (1991) first considered whether another right-lateral fault might cut through part of Durmid Hill, southwest of the mSAF, because he observed hinge zones of almost east-trending folds that change to northwest trends as they approach the Salton Sea from the east. This geometry is in mirror image to their change in trend near the mSAF. Bürgmann (1991) recognized that a right-lateral fault near the Salton Sea could explain the anomalous northwest trends of the fold hinge lines in Durmid Hill, but until our study, no faults were mapped there (Fig. 2; Bürgmann, 1991; Babcock, 1974; Dibblee, and Minch, 2008a, 2008b, 2008c; Janecke and Markowski, 2013a, 2013b, 2015a, 2015b, 2016; Markowski, 2016).

Geologic Framework

The SAFZ and related structures cut a variety of Pliocene to modern lacustrine, playa, fluvial, and eolian sedimentary rocks between North Shore and Bombay Beach (NS and BB in Fig. 3; see also Fig. 4; Dibblee, 1954, 1997; Babcock, 1974; Bürgmann, 1991). These rocks contain few datable horizons and display significant lateral and vertical variations in lithology, facies, and provenance. This makes deciphering the basic stratigraphy of the Durmid Hill area quite challenging in highly faulted areas. Fortunately, the rock units share key diagnostic features with Neogene and Holocene formations of the western Salton Trough, and we correlated them with their much-less-deformed and better-dated equivalents on the southwest side of the Salton Sea by using their diagnostic characteristics. These included the presence of large sand-filled desiccation fractures, bedded gypsum, distinctive siliceous pebbles, several kinds of concretions, diverse subaerial facies, and a mixture of L and C suite sands (Fig. 4; Kirby et al., 2007; Janecke et al., 2010a, 2010b; Dorsey et al., 2011).

Dibblee (1954, 1997) and Dibblee and Minch (2008a, 2008b, 2008c) originally assigned all of the rocks southwest of the SAFZ to the Pliocene–Pleistocene Borrego Formation based on the presence of abundant mudstone, but Dibblee (1954) commented that the rocks also resembled the overlying Pleistocene Brawley Formation (Fig. 4). Babcock (1974) identified an ash in the sedimentary section that was later correlated to the 0.765 ± 0.008 Ma Bishop Ash (Izett et al., 1988; Sarna-Wojcicki et al., 2000; Zeeden et al., 2014). The Bishop Ash intertongues with type areas of the Middle and Upper Pleistocene Ocotillo and Brawley Formations southwest of the Salton Sea (Fig. 4; Lutz et al., 2006; Kirby et al., 2007; Herzig et al., 1988), yet correlations of ash-bearing sedimentary rocks in the Durmid and Mecca Hills were not revised upward from Borrego Formation to the age- and facies-equivalent Brawley Formation until Markowski (2016) and this study. Discovery and characterization of the Thermal Canyon Ash, up section from the Bishop Ash, further confirms the correlation with the Brawley Formation (Markowski, 2016). Lacustrine mudstone and sandstone dominate the Brawley Formation, and its fluvial, eolian, and playa facies, which include meter-deep, sand-filled desiccation cracks and abundant bedded gypsum, are diagnostic of the Brawley Formation (Fig. 4; Kirby et al., 2007; Markowski, 2016).

The northern Salton Sea and most of Coachella Valley, southwest of the SAFZ, form a monocline of latest Pleistocene to Holocene beds that dip

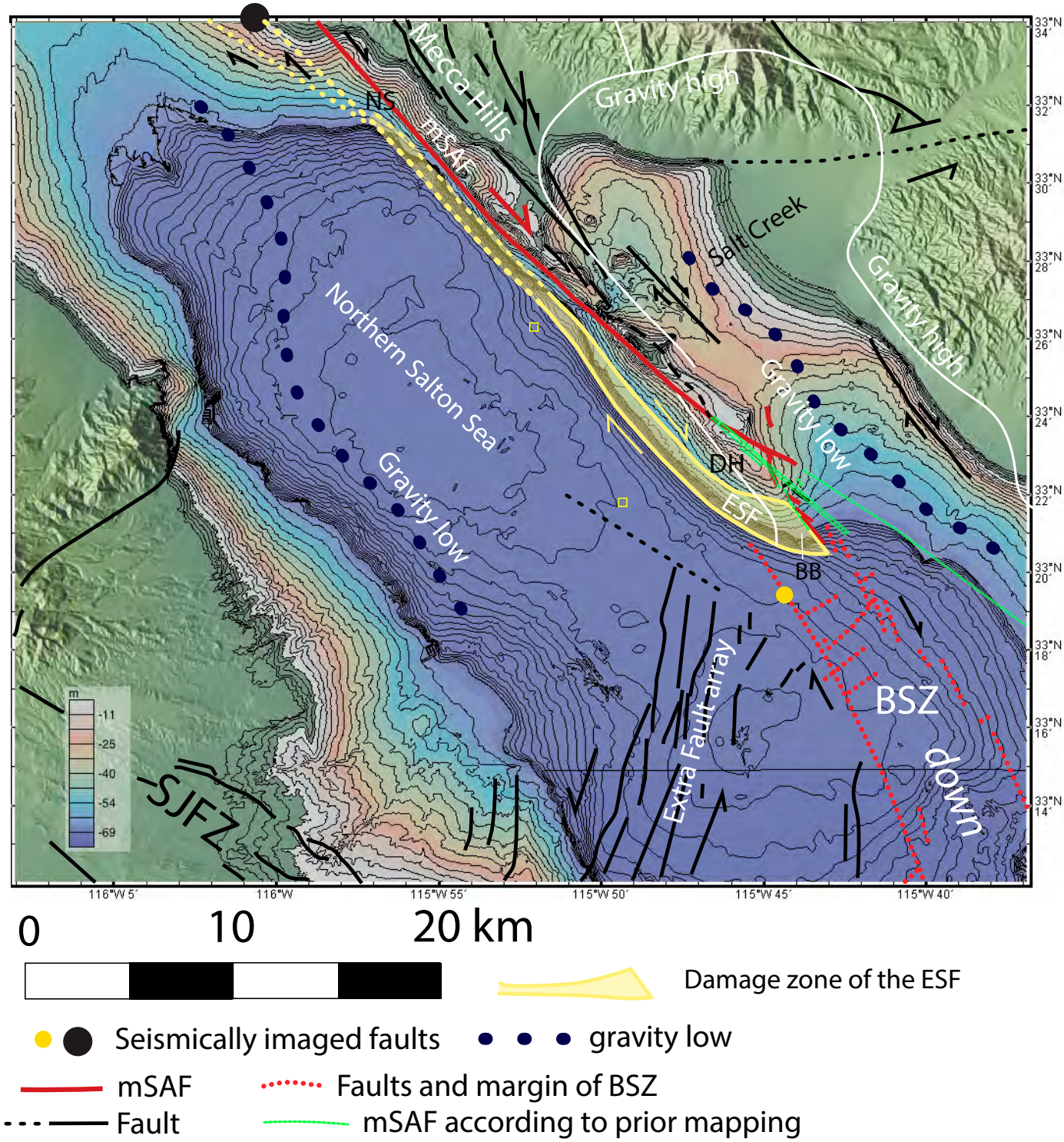

Figure 3. Digital elevation model with 5 m contours showing how the shape of Durmid Hill (DH) and the Salton Sea (1 m contours) are strongly controlled by the ESF and to a lesser extent, by the mSAF between North Shore (NS) and Bombay Beach (BB). Yellow lines are the approximate NE and SW edges of the ESF, and red lines are our mapped traces of the mSAF. The bunched up topographic contours within the ESF match the overall trends and strikes of folds, faults, and beds within the ESF, and contours separate farther southwest on the flat floor of the Salton Sea. The southwest edge of the ESF is probably related to the pronounced break-in-slope along the eastern margin of the Salton Sea. The mSAF (red), in contrast, cuts across topographic lows and high, particularly south of Salt Creek. Topography changes significantly southeast of Bombay Beach as the Durmid ladder pinches out and transitions into the BSZ across a large area. Prior workers disagreed about the location, strike, and geometry of the mSAF north of Bombay Beach (compare the green lines from Babcock, 1974, and Clark, 1984). Gravity lows (dark blue dotted lines) and local gravity highs (white lines) indicate that the southern part of the Durmid ladder structure is uplifted (Langenheim et al., 2014). See Figure 1 for location of this map. Reflection seismic profiles of Sahakian et al. (2016) are uninterpretable due to gas east of the yellow squares.

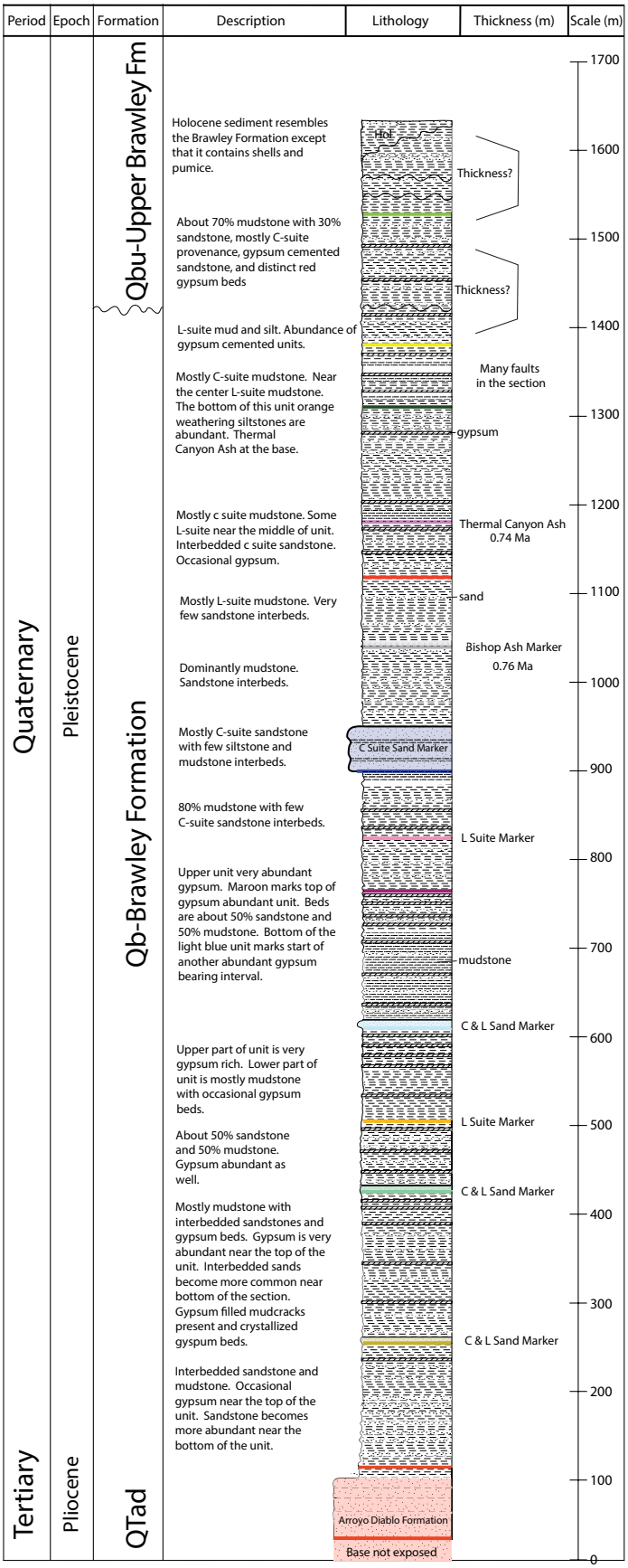

Figure 4. Stratigraphic column of the Pliocene–Pleistocene Brawley Formation in Durmid Hill. Updated and modified from Babcock (1974). The uppermost Arroyo Diablo Formation is present at the base. Its age is Pliocene, southwest of the Salton Sea (Dorsey et al., 2011). See Markowski (2016) for the techniques used to construct this composite column and for a map of colored markers.

northeast toward the SAFZ (Dorsey and Langenheim, 2015; Sahakian et al., 2016). The SAFZ in Coachella Valley also dips northeast (e.g., Nicholson, 1996; Fuis et al., 2017) and has a small reverse component of slip. Most workers agree that transpression dominates the area and causes the exhumation of large volumes of basin fill in the SAFZ (Babcock, 1974; Bilham and Williams, 1985; Bürgmann, 1991; Lindsey and Fialko, 2013; Lin et al., 2007; Lin, 2013; Fuis et al., 2012; Fattaruso et al., 2014; Tong et al., 2014), although some workers disagree and propose that transtension dominates throughout the Salton Sea area (Brothers et al., 2009, 2011; Sahakian et al., 2016).

METHODS

We mapped the southern 15 km of the SAFZ in Durmid Hill in detail and made numerous traverses through the less-exhumed and the less-well-exposed 15 km of the fault zone directly to the northwest. Salt Creek separates these two areas, and we refer to the area southeast of Salt Creek as Durmid Hill, and to the area northwest of Salt Creek as the Corvina section, for Corvina Beach at its midpoint (Figs. 1 and 2). In Durmid Hill, geologic maps at a range of scales, structural and stratigraphic studies, two sets of light detection and ranging (LiDAR) scenes (B4 project [Open Topography, 2005]; Salton Sea LiDAR Collection, 2010), false- and natural-color aerial photography, and published seismic and gravity data reveal the detailed evolution of structures within the southern 15 km of the SAFZ (Markowski, 2016; this study). Transects through the less-continuous exposure in the Corvina section show that the same structural style persists along the entire northeast margin of the Salton Sea and forms an ~25–30-km-long ladder structure (Fig. 2).

Field studies in the low-topographic-relief area of Durmid Hill benefited from the multiple years of high-resolution natural-color aerial imagery available in Google Earth, false-color digital scenes created from 3 or 4 bands of the National Agriculture Imagery Program (NAIP), national high-resolution (15 cm) imagery, Landsat 7+ imagery (15-m-scale resolution), topographic data sets in GeoMapApp, bathymetric contours of the floor of the Salton Sea (Redlands Institute, 1999), relocated earthquakes (Hauksson et al., 2012), geodesy (Tong et al., 2013; Lindsey et al., 2014), and gravity data sets (Langenheim et al., 2014). Additional published refraction and reflection seismic, magnetic, and gravity data sets, tomographic models, relocated earthquakes from the Southern California Earthquake Center database (http://scedc.caltech.edu/), and geodetic data allowed us to further refine our interpretations (Babcock, 1969; Shearer et al., 2005; Brothers et al., 2009, 2011; Tong et al., 2013; Lin, 2013; Lindsey et al., 2014; Langenheim and Powell, 2009; Hauksson et al., 2012; Dorsey and Langenheim, 2015; Langenheim et al., 2014; Fuis et al., 1984, 2012, 2017; Barak et al., 2015). Results of the Salton Seismic Imaging Project clearly imaged the geometry of the SAFZ in the subsurface and confirmed our interpretation of the northward continuation of the East Shoreline fault (ESF) basinward of both the Mecca and Indio Hills (Hernandez et al., 2015; Fuis et al., 2017).

We used false-color, four-band digital aerial photography to clarify the geometry of faults, marker beds, and folds in the SAFZ. False-color processing techniques adapted from Dohrenwend et al. (2001) highlighted marker units with compositions that differed from those of the enclosing sedimentary package (Figs. 2 and 4). Vegetation lineaments localized

along fault zones provided additional key information about fault traces in this hyperarid environment.

High-resolution imagery is key for locating discordant structures suitable for focused field study (Fig. 5). Many strike-slip and oblique-slip faults are bedding-strike–parallel and bedding-plane–parallel features. Lateral and downdip ramps, and folds highlight short sections of cryptic faults. Therefore, fault-bend folds were a powerful tool for locating subtly expressed strike-slip faults. Identification of lateral and frontal ramps along the hundreds of strike-slip faults in the SAFZ is critical in mapping faults through what could otherwise appear to be intact stratigraphy.

The persistent seismicity in the BSZ delineates the locations, depths, dips, and northeast to east-northeast, north, and north-northwest strikes of faults (Shearer et al., 2005; Lin, 2013). We used the most current earthquake catalogs of Hauksson et al. (2012, 2017) to plot precisely relocated earthquakes near our study area (Fig. 1). Alignments of earthquakes provided insights into the geometry of the boundary zone between the SAFZ and the northernmost BSZ (Fig. 1).

RESULTS

Overview

Our multidisciplinary study within the SAFZ revealed the existence of a >30-km-long, and several-kilometer-wide, Durmid Hill ladder-like fault zone that has the well-known mSAF on its northeast edge and the newly identified ESF on its southwest edge (pink and yellow shaded areas, respectively, in Fig. 2; Markowski, 2016). In Durmid Hill, highly faulted and intensively folded, uppermost Miocene (?) to modern sedimentary rocks are being exhumed between the northeast side of the Salton Sea and the mSAF (Fig. 2). Our new geologic map reveals a myriad of closely spaced, brittle to semibrittle faults within Durmid Hill that form an organized mesh of right- and left-lateral strike-slip faults. Altogether, the main and newly identified East Shoreline right-lateral faults are part of a single ladder-like fault zone that is typically 1–3 km wide and at least 30 km long. North of the Salton Sea, there is no evidence

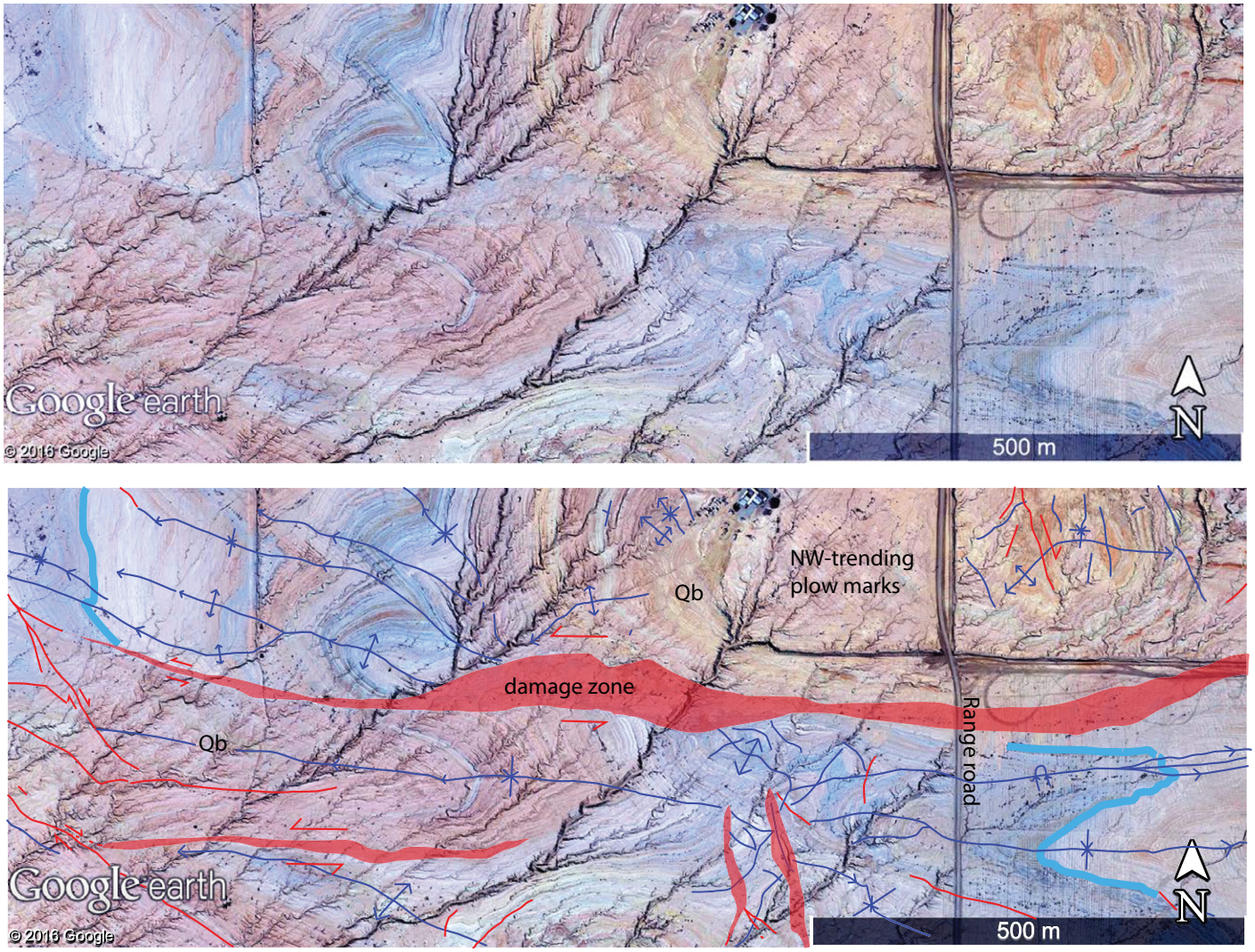

Figure 5. Uninterpreted (above) and interpreted (below) false color aerial photograph of some cross faults in the Durmid ladder structure. Both narrow (red lines) and wide (red polygons) left-lateral strike-slip faults connect the two strands of the SAFZ that are adjacent to this scene. The thick light blue lines highlight a key marker bed in the Brawley Formation that is displaced ~ 1 km by an east-striking fault. Notice how many of the most laterally continuous fold axes (dark blue lines) roughly parallel the fault zones. The syncline that intersects the word "road" follows along the widest left-lateral fault zone for ~ 1 km. Qb—Brawley Formation. See Figure 2 for location.

that the right-lateral master faults interact by means of closely spaced cross faults (Fig. 1).

Active left- and right-lateral cross faults between the master faults have a geometry reminiscent of the rungs of a sheared ladder and contribute to the transpression and uplift throughout the SAFZ. The Durmid ladder structure is named for its clearest expression on the southwest flank of Durmid Hill (Fig. 2). It trends ~310°–315° there, and overall its perimeter resembles a southward-pointing sword along the southeastern side of the Salton Sea (Figs. 1 and 2). The two master right-lateral faults converge in shallow water southeast of Bombay Beach, where the SAFZ changes across a transitional zone into the BSZ. North of the Salton Sea, erosion and latest Holocene sediment related to the 1905–1907 Salton flood and Lake Cahuilla obscure so much of the ESF at the ground surface that we relied more heavily on subsurface data sets there (Table 1; see following). Each of the faults in the Durmid ladder structure has its own wide damage zone.

We documented the structural elements that comprise the Durmid ladder structure, starting with the right-lateral and right-oblique faults along its margins. We focused particular attention on the character and significance of the newly identified structures, such as the ESF of the SAFZ along its southwest margin, and the cross faults and folds within it. The structural geometry of the mSAF changes significantly along its southernmost 6–10 km, and we contrast this zone with its simpler traces farther north. We first describe what is known about the transition between the SAFZ and the BSZ in the south, and then we briefly explore the persistence of the ESF of the SAFZ along strike to the northwest.

Spaced left-lateral cross faults are characteristic of the southern 30 km of the SAFZ and the entire BSZ, farther south along the plate boundary (Fig. 1). These shared structural geometries are unexpected, because the plate boundary changes from persistently transpressional to persistently transtensional between these two fault zones. Rocks on either side of the Durmid ladder structure are less deformed than those within the fault zone, and their structural and stratigraphic relationships shed light on the intensity of deformation within the SAFZ.

Cenozoic Stratigraphy

The stratigraphy of deformed rocks in Durmid Hill has to be documented in order to correctly map the structural geology of the SAFZ. The bulk of the area is underlain by deformed Brawley Formation (Fig. 4). Thick freshwater perennial lake deposits of the Borrego Formation are absent, and at the deepest stratigraphic levels on the west side of the mSAF, we identified the Arroyo Diablo Formation (Figs. 2 and 4; Markowski, 2016), which is a thick interval of sand-rich beds dominated by iron-stained, orange-weathering sand derived from the Colorado River (Dibblee, 1954, 1984; Winker, 1987; Dorsey et al., 2011). The concretion-bearing uppermost part of the Arroyo Diablo Formation forms the core of two significant faulted anticlines in central Durmid Hill and occurs in discordant slices of numerous small fault blocks in northern Durmid Hill (Figs. 2 and 4). It contains rare conglomerate beds with well-rounded siliceous clasts that are diagnostic of the Arroyo Diablo Formation. Mudstone and sandstone of the Brawley Formation coarsen northward into grit and conglomerate-bearing beds of the Ocotillo Formation ~1 km south of Salt Creek (Markowski, 2016).

The even older (?) Shavers Well Formation is faulted up in an elongated horst block northeast of the mSAF, from 33.5°N (about at the southern limits of North Shore, California) to a point along the mSAF that we call the bushy seeps (33.4076°N; Figs. 1 and 2; Babcock, 1974). The age and stratigraphic position of the Shavers Well Formation are ambiguous because it lacks stratigraphic contacts with dated strata. North of Salt Creek, it appears to transition up section from locally derived clastic sediment to a mix of local and Colorado River–derived deposits. If those local and Colorado River–derived deposits correlate with the base of the Arroyo Diablo Formation and the Palm Springs Group, then the Shavers Well Formation could be a subaerial equivalent to the Imperial Group, and therefore it could be as old as latest Miocene (Sylvester and Smith, 1976; Winker, 1987; Steely, 2006; Dorsey et al., 2007, 2011). Prior workers, however, inferred a Pliocene–Pleistocene age on the basis of lithologic correlations (Babcock, 1974). Body fossils are lacking, and better age control is needed.

Main Strand of the San Andreas Fault

The mSAF in Durmid Hill is the simplest part of the Durmid ladder structure. In the northern half of the detailed study area, for 7 km south of Salt Creek, the mSAF consists of one or two simple traces. It consistently lies on the northeast edge of a highly faulted, and internally folded damage zone that pinches and swells, but it is typically several hundred meters across and southwest of a fault block of Shavers Well Formation (Figs. 2 and 3). From North Shore, California, to the bushy seeps, the mSAF separates a fault block of folded and faulted Miocene(?)–Pliocene Shavers Well Formation strata on its northeast side from strongly folded and faulted, Pliocene–Pleistocene Ocotillo and Brawley Formations, and Pliocene(?) Arroyo Diablo Formation strata on its southwest side (Figs. 2 and 6; Babcock, 1974; this study). The fairly consolidated and cemented Shavers Well Formation forms a linear ridge that parallels the mSAF (Fig. 3).

The mSAF changes from a simple fault trace in the north to a complex southern geometry starting at the bushy seeps (labeled in Figs. 2 and 6). There, the mSAF splays, broadens, and steps onto several strands that have a complex horsetail map pattern. The increased intensity of faulting at branch points localizes seeps, small bushes, trees, and coppice dunes at the boundary between the simple northern and complex southern branches of the mSAF (Fig. 6). The identity of the main, most active traces is much less certain southeast of the bushy seeps, because its traces mostly juxtapose the Brawley Formation against the Brawley Formation. The Shavers Well Formation is nearly absent, except in fault slivers <20 m across.

Fractures that formed during creep and triggered slip are present discontinuously all along traces of the mSAF from North Shore to 1.5 km northwest of Bombay Beach. These fractures allowed us to locate previously unmapped fault traces and to identify the more active ones among the southern branching traces of the mSAF (Fig. 6). South of the bushy seeps, the main strand first splays and steps into several strands that diverge southward. Even farther south, some traces bend to northerly strikes, others have en echelon steps, and a few faults change into mini-ladder structures or give way to poorly understood complexities and a dispersed fault zone. Many strands are difficult to trace because they drop in elevation into lower terrain with Holocene cover around the edge of the Salton Sea. The detailed geometry of the southern 5 km of the mSAF is emerging as we continue to sort out the extent of angular unconformities and other complexities there (Fig. 2).

Damage Zones Along the Main Strand of the San Andreas Fault

The damage zone of the mSAF is many hundreds of meters wide, is laterally continuous, and has a persistent and strong asymmetry. The most strongly folded and faulted part of the damage zone is localized on its southwest side, where it has a map-scale block-in-matrix texture (Fig. 6). Babcock (1974) and Bürgmann (1991) also described this damage zone as a highly sheared fault zone along the mSAF. Rocks on the northeast side of the active creeping trace of the main strand are much more intact

TABLE 1. EVIDENCE FOR THE DURMID LADDER STRUCTURE AND THE EAST SHORELINE FAULT ZONE (ESF) ALONG ITS SOUTHWEST EDGE

Location and nature of evidence	Figure	References
Near and within the East Shoreline fault zone		
There are many tens of northwest-striking, right-oblique and right-lateral faults within the ~1-km-wide damage zone of the ESF	2, 7, 8A, 8B, 9, 10, and 12	Markowski (2016), this study
Northwest-striking, right-oblique and right-lateral faults are uncommon on either side of the ESF	1, 2, 3, and 14	Markowski (2016), this study, Sahakian et al. (2016)
Shortening produces monoclines, synclines, and anticlines in the ESF that are counterclockwise of its faults by less than ~10°	2, 7, 9, and 12	Markowski (2016), this study
Uplift is occurring within the ESF due to faulting and folding, and this process is exhuming several members of the main and upper Brawley Formation	1, 2, 7, 9, 10, 12, and 15	Markowski (2016), this study
Faults and fractures within the ESF cut Pleistocene, upper Holocene, and modern sediment	2, 7, 8, 9, 10, 11, 12, 14	Markowski (2016), this study
Progressive deformation occurs in the ESF and that has produced several angular unconformities	9, 10	Markowski (2016), this study
Active subsidence is ongoing beyond the southwest edge of the ESF, beneath the northern Salton Sea	1, 2, 3, 14, and 15	Sahakian et al. (2016), this study
The curvature of the steeper, easternmost floor of the Salton Sea closely parallels the curvature of the mapped faults, folds, and beds of the ESF	2 and 3	This study
The ESF is well expressed, active, and marked by long, narrow, linear, hairline fractures in all types of modern sediment along ~18 km of the beach northeast of the northern Salton Sea.		Janecke (2013), Janecke and Markowski, (2013, 2015a, 2015b, 2016), Markowski (2016), Janecke et al. (2016)
Most linear fractures occur within fault zones, where their existence can be determined independently		Markowski (2016), Janecke and Markowski (2013, 2015a, 2015b 2016), Janecke et al. (2016)
Within the domain of cross faults		
Left- and right-lateral cross faults connect the ESF and the main strand of the San Andreas fault zone (mSAF) like rungs on a ladder	1, 2, 5, 14, 16, and 17	Markowski (2016), this study
Faults in cross-fault domain change their strike into near-parallelism with the ESF as they approach it	2, 14	This study
Fold axes in the east-striking cross-fault domain change their trends 10°–20° in a clockwise sense as they approach the ESF and mSAF	2; Table 1	Babcock (1974), Bürgmann (1991), Markowski (2016), this study
Uplift is occurring within the cross-fault domain that exposes units as old as the Pliocene Arroyo Diablo Formation	2, 4	Markowski (2016), this study
Fault blocks in the left-lateral part of the cross-fault domain are up to 55° clockwise of their original and ideal geometry	2, 5, 14, 16	Markowski (2016), this study
Markers displaced 500–1250 m left-laterally across cross faults restore by removing ~55° of clockwise rotation	5, 16	This study
Uplift and subsidence patterns determined by geologic and structural mapping have a close match to ones measured in interferometric synthetic aperture radar (InSAR)		Tong et al. (2013), Lindsey et al. (2014), Markowski (2016), this study
A gravity high shows that the southern half of the Durmid ladder structure is an uplifted fault block between the mSAF and ESF, in agreement with the structural data	2, 3	Langenheim et al. (2014), this study
From the Salton Sea		
The youngest beds southwest of the San Andreas fault zone dip directly toward the Durmid ladder structure	15	Dorsey and Langenheim (2015), Sahakian et al. (2016)
A prominent break in slope in the shallow water of the Salton Sea probably coincides with the southwest edge of the ESF because deformed Pleistocene rocks persist into the shallow Salton Sea yet no faulting or folding was imaged offshore	3 and 12	Bathymetry of Redlands Institute (1999), Sahakian et al. (2016), this study
Northeast edge of Coachella Valley		
Exhuming Pleistocene basin fill in the basin block of the southwestern Mecca Hills indicates a large fault block is uplifting between the mSAF and the buried northward continuation of the ESF	1	Rogers (1965), Sylvester (1988), Dibblee and Minch (2008b), this study
Exhuming Pleistocene basin fill in a fault block in north Indio, California, at Desert Park, lies southwest of the mSAF and northeast of a buried right-lateral fault that we correlate with the northern continuation of the ESF, and the uplifting block is about 2.5 km by 0.8 km	1	Rogers (1965), Petra Geoscience, Inc. (2009)
Migrated reverse-moveout reflections from the southwest edge of the Mecca Hills imaged northeast-dipping surfaces of the along-strike continuation of the ESF	Dot in 1 and 3	Fuis et al. (2017)
Migrated reverse-moveout reflections south of the Indio Hills in northern Coachella Valley (line 5) show numerous steep, northeast-dipping fault surfaces in a 5-km-wide zone that we tentatively correlate to the along-strike continuation of the ESF and the Garnet Hills fault zones	Dots in 1	Hernandez et al. (2015), this study
The ~1–5-km-wide strip southwest of the Indio Hills has unique hydrologic characteristics that distinguish it from the bulk of Coachella Valley, and this subarea is bounded by the projection of the Garnet Hill fault toward Desert Park	1	California Department of Water Resources (1964)
Uplifted basin fill is dipping toward Coachella Valley in all red blocks of Figure 1, in the opposite direction of the beds beneath the floor of Coachella Valley	1	Sylvester and Smith (1976), Dibblee (1997), Petra Geoscience, Inc. (2009), Dorsey and Langenheim (2015), Hernandez et al. (2015), Markowski (2016), this study

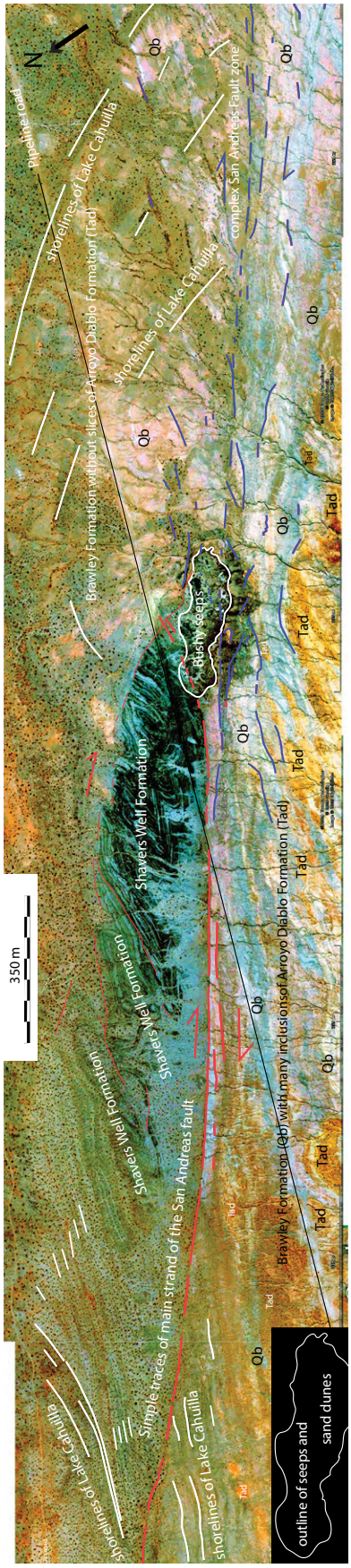

Figure 6. Strip map showing the simple trace of the mSAF (red) in the northwest where it separates the Shavers Well Formation (blue-black colors) and the multicolored Brawley Formation with fault blocks of the Arroyo Diablo Formation (orange) enclosed in a disrupted block-in-matrix type of damage zone. Creep is localized on this single strand of the mSAF (Lindsey et al., 2014). Starting at a group of seeps that produced bushy coppice sand dunes (white outline), the mSAF splays southeastward. We refer to this area as the bushy seeps (BS). The mSAF is blue where several traces diverge. Gravel beach ridges formed by Lake Cahuilla (white lines) are plentiful on the northeast side of the mSAF and much less common on its southwest side, in the Durmid ladder structure. Base map is a false color Google Earth scene from 2005. Each distinct color coincides with a unique rock type. Tad—Arroyo Diablo Formation; Qb—Brawley Formation. See Figure 2 for location.

than the extremely faulted and folded rocks in the damage zone on the southwest side of the fault (Figs. 2 and 6).

The most-damaged rocks southwest of the mSAF are continuous from Salt Creek to ~3 km north of the Salton Sea. The damage zone is so strongly deformed that the protolith of the damaged rocks is difficult to identify with certainty (Figs. 2, 5, and 6) due to the block-in-matrix texture and submeter scale of the largest blocks in the damage zone (Fig. 6). The fault map in Figure 6 illustrates some of the extreme deformation and mix of lithologies that occur as the damage zone grades from containing identifiable fault-bounded blocks of distinct sedimentary rocks to thoroughly mixed rock types. The zone of strong damage with a block-in-matrix texture is typically 200–300 m wide along the mSAF, but it becomes less regular and wider where mud-rich rock units dominate (Fig. 2). The boundaries of the damage zone are most ambiguous where the SAFZ bends and where the damage anastomoses around lozenges of more intact rock (Fig. 2). A less intensely deformed damage zone on the northeast side of the mSAF (Fig. 2) is composed of many closely spaced fault-fold pairs.

Stratigraphic juxtapositions and gravity data show that the mSAF changes from having a northeast-side-up component of vertical deformation south of Salt Creek to having a northeast-side-down component near the Salton Sea (Babcock, 1969; Langenheim et al., 2014; Markowski, 2016). In addition, the southern 3–5 km section of the mSAF zone and its damage zone become more complex closer to the Salton Sea, and Holocene cover becomes widespread within the fault zone. The southern 5 km section of the mSAF appears to consist of an incompletely understood, southward-widening, triangular ladder-like fault zone (Fig. 2). The northeast margin of the triangular zone is close to the queried traces of the mSAF of Hope (1969), Babcock (1974), and Jennings (1967), whereas its western traces are closer to the fault traces mapped by Dibblee (1954, 1997) and Clark (1984) (yellow and black fault traces in Fig. 3).

This triangular ladder resembles parts of the Durmid ladder structure in that it is internally deformed and has many cross faults, but it also resembles the BSZ, to the south, with its subdued topographic expression, subsidence, widespread Holocene deposits, and north-striking normal-oblique faults. Much more structural analysis and mapping are needed to document this part of the mSAF.

East Shoreline Strand of the San Andreas Fault

The East Shoreline strand of the San Andreas fault (ESF) is a right-lateral zone of faults and folds that has a southwest-down vertical component of slip and ranges from <0.5 to >1 km wide (Figs. 2 and 7). The existence of the ESF was first confirmed from exposures in the many gullies east of the Salton Sea (Figs. 2, 8, 9, 10, and 11; Markowski, 2016). Mapping, field studies, and structural analysis show that it has right-lateral and right-oblique faults and folds within it. There are some dip-slip faults and flexural slip along bedding planes. No single fault dominates the wide fault zone, and, instead, numerous right-lateral and right-oblique fault zones combine with folds to form a band of displaced and damaged rock on the northeast shore of the Salton Sea. Growth relationships indicate that deformation and faulting were coeval during deposition of the upper Brawley Formation (Figs. 9 and 10; Markowski, 2016).

In order to clearly document that the Durmid ladder structure is the SAFZ, we enumerate the key evidence for its existence, geometry, kinematics, and width in Table 1. Evidence for active deformation and displaced modern sediment of the ESF was briefly discussed in Markowski (2016), Janecke and Markowski (2013, 2015a, 2015b), and Janecke et al. (2016). Fractured modern sediment is so common and widespread in the fault zones of the Durmid ladder structure that it will be explored elsewhere (for a preview, see Markowski, 2016; Janecke et al., 2016).

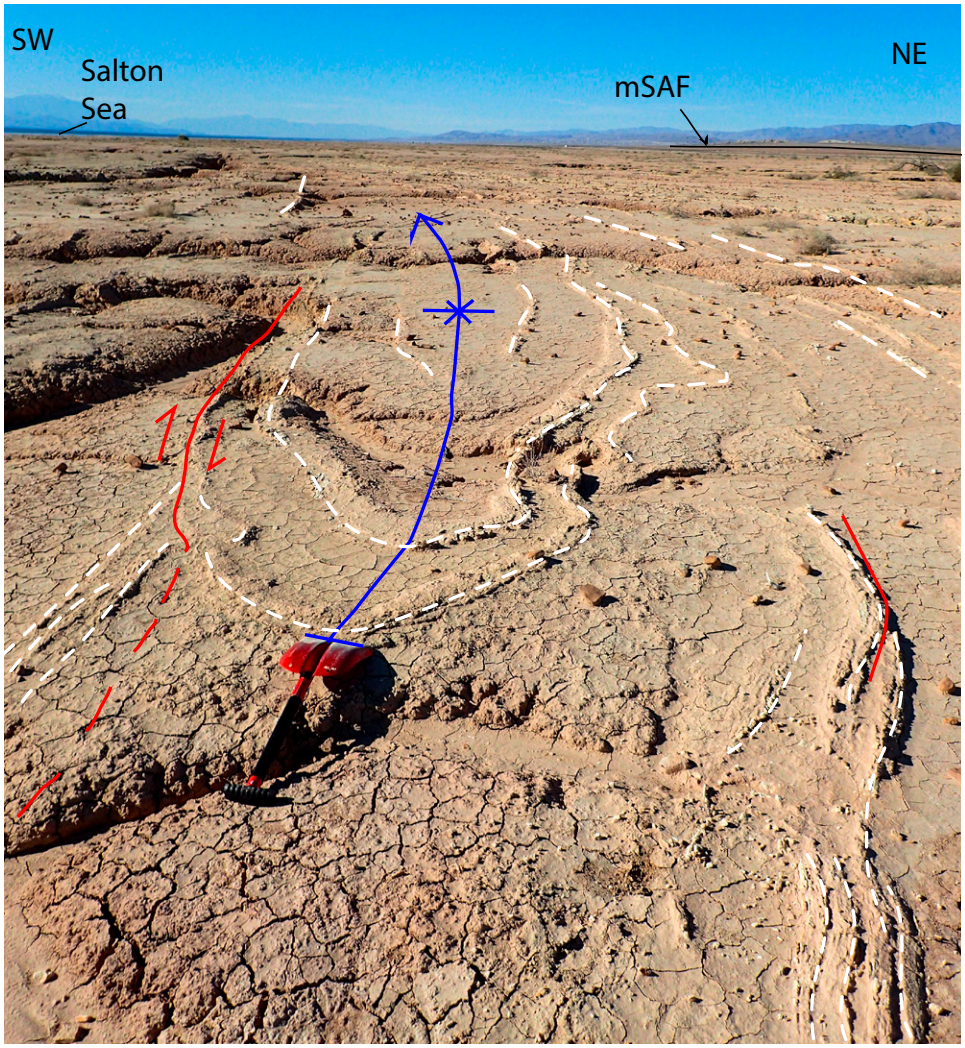

Figure 7. Photograph of a typical fault-fold relationship within the ESF zone in down-plunge view. View of a northwest-plunging syncline of Brawley Formation that is grossly parallel to a right-lateral fault along its southwest limb (red). The shovel is 80 cm long. See Figure 2A for location. White dashes lines are bedding traces.

The ESF contains many tens of steeply to moderately dipping, northwest-striking, right-lateral faults that both cut out and repeat Pliocene to Holocene strata and produce growth relationships that include progressive unconformities across <100 m lateral distance (Table 1; Figs. 2, 8A, 8B, 9, 10, and 11). Monoclines, synclines, and anticlines that formed in close association with these right-lateral strike-slip faults in the ESF commonly follow along the curving northwest-striking faults for distances up to 3 km (Figs. 2 and 7). Within the fault zone, many short- to moderate-length, northwest-striking, right-lateral and right-oblique faults occur with variable spacing and variable lengths, and these gradually change their strikes in the southern part of Durmid Hill to more westerly orientations (Fig. 2). The strikes of beds, trends of folds, and the contours of the landscape also curve and grossly parallel the fault zone. The many subparallel faults and folds of the ESF consistently produce a damage zone that is at least 1 km wide. At the eastern edge of Bombay Beach, the ESF zone ends and merges with the mSAF. The Brawley Formation dominates the ESF, except south of Salt Creek, where granule conglomerate beds of Ocotillo Formation replace the finer Brawley Formation. The ESF curves and has strikes between 280° and 320° along Durmid Hill, with strikes in the 310°–315° range being most common.

North of Salt Creek, widespread Holocene cover obscures the ESF, and the midline of the fault zones is centered on the modern beach instead of being centered between Durmid Beach and Highway 111 (Figs. 1, 2, 5, 8, and 9). The fault zone is narrower in this section than it is farther south (Fig. 1).

Faults in the ESF typically parallel the strike of bedding, except in lateral ramps that connect adjacent bedding-strike–parallel parts of the faults (Figs. 8, 9, 10, and 11). The quasi–en-echelon faults are typically vertical to steep, although there are some parts of the right-oblique fault zones with moderate to low dips. The faults in the ESF zone cut Pleistocene and Holocene beds, cut out and repeat strata, have similar strikes as northwest-trending synclines, anticlines, and monoclines in the fault zone, and have produced a variety of growth folds (Figs. 7, 9, and 10). Although some faults are narrow planar surfaces, most deform and damage rock across many meters perpendicular to strike (Figs. 8, 9, 10, and 11). It is common for faults to occur in clusters, and this makes it difficult to identify the trace with the most displacement.

Slickenlines on fault surfaces, when preserved, reveal complex slip patterns. Two or more distinctly different rakes are common in the faulted mudstones along individual fault surfaces, on surfaces within one fault zone, and from one fault to the next. The proportion of strike-slip, oblique-slip, and dip-slip slickenlines varies significantly across the field area, and we did not observe enough slickenlines to make sense of this complexity. It is clear, however, that there is a mixture of slip directions in every

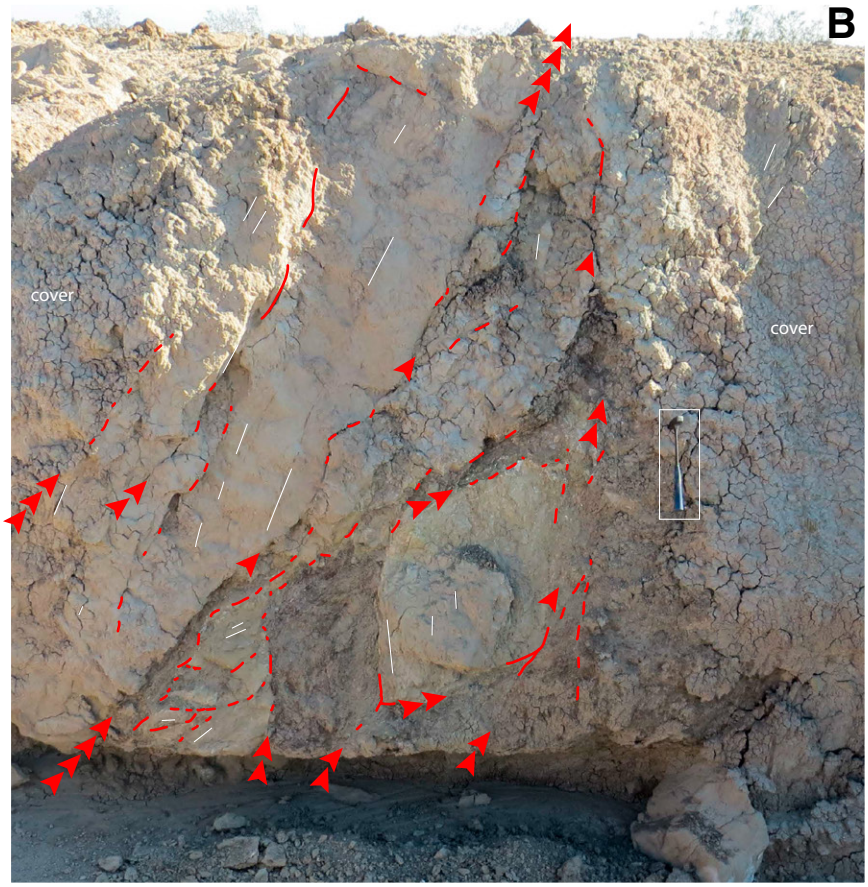

Figure 8. Fault zones exposed in the ESF. (A) View to the southeast of a right-reverse fault zone of the ESF near highway 111. Dark mudstone of the Brawley Formation is parallel to several of the faults in this wide damage zone. Notice the folded sandstone beds within the fault zone. Arrows point to faults and red lines map them. White lines define selected traces of bedding. This exposure is ~1.25 m high. (B) View to the southeast of a right-reverse fault zone cutting the Brawley Formation within the ESF. Note the rock hammer for scale. The lighter beds are sandstone beds with feldspathic compositions and local sources. Red to brown mudstone is highly sheared and encloses more intact fault blocks of sandstone in the damage zone of this fault. Traces of bedding are white lines. Arrows and red lines denote faults. See stars in Figure 2 for locations. Both fault zones have top-to-the-SW components of deformation.

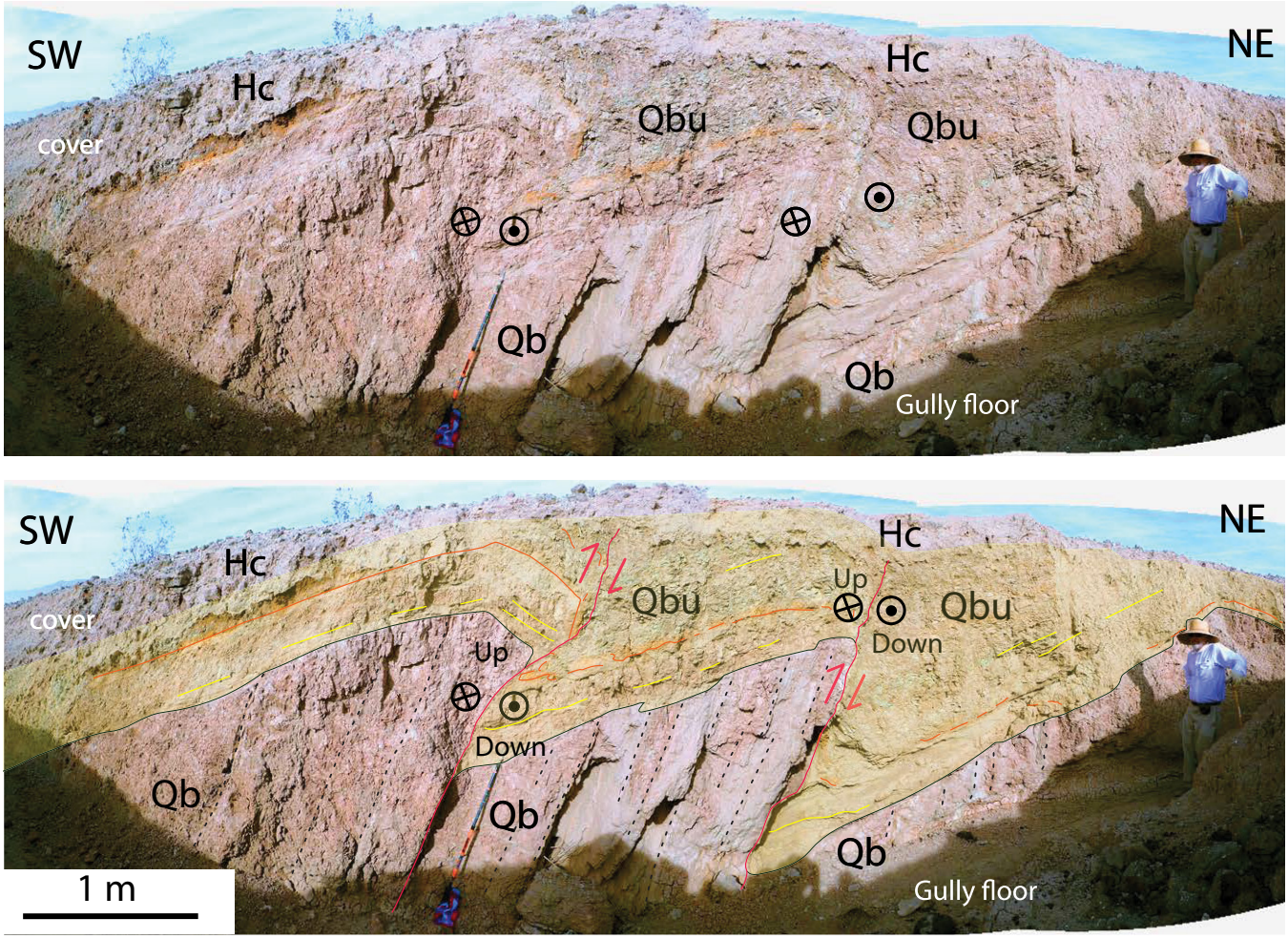

Figure 9. Annotated photograph with (below) and without structural interpretations (above) showing a faulted angular unconformity that formed during growth faulting along the eastern margin of the ESF. This zone expresses transpression. Less deformed Holocene and Pleistocene Upper Brawley Formation (Qbu) lies in angular unconformity on steeply southwest-dipping Lower Brawley Formation (Qb), and both are displaced by faults in the ESF. The ~ 0.5 to 1.5 m of reverse-separation across each fault occurs along a fault that has a flat-on-flat geometry below the unconformity. Dip-slip slickenlines are more plentiful than oblique-slip or strike-slip slickenlines, and there may be strain partitioning in this top-to-the-northeast fault zone. Several other faults are outside the view. Hc—latest Holocene to modern cover. Dashes define bedding traces below the unconformity, whereas yellow lines are above it. The orange line is an iron-rich marker bed. See Figure 2 for location.

fault zone that preserves them. While these observations complicate the interpretation, the steep to vertical geometry of many faults suggests that strike-slip deformation is dominant.

Folds in the East Shoreline Fault Zone

The orientations of axial surfaces of monoclines and plunging synclines and anticlines within the fault zone are similar to the overall strikes of the right-lateral strike-slip faults in the ESF zone (Fig. 2). Individual folds persist subparallel to faults for long distances, and the longest fault-fold pair is ~3 km long (Fig. 2). The 0–15° angles between trend of fold-hinge zones and the strikes of adjacent faults are much less than the ~45° angle predicted by bulk simple shear (Figs. 2C and 2D; Sylvester, 1988). The dominant fault-subparallel sets of folds have predictable and regular geometries at the map scale. Weak beds and disharmonic décollement-style folding here and there produce chaotic subsidiary folds as well.

The ESF zone is a dispersed zone of many fault-fold pairs. At the surface, it slices through the mudstone-rich and gypsum-bearing Pleistocene Brawley Formation. The age of the formations is generally younger toward the ESF, and some of the youngest units of the field area are in and adjacent to the ESF zone.

The right-lateral faults and folds throughout the ESF zone represent a distributed damage zone that lacks a fault core. The width of this damage zone varies somewhat as cross faults merge into it from the east (Figs. 2B and 2C). In places, damage spans up to 1 km (Fig. 2A). In contrast to the damage zone southwest of the creeping and localized mSAF, farther east, beds are intact at the map scale in the ESF zone, and disrupted rocks of the block-in-matrix type occur only in the fairly narrow fault zones of the East Shoreline fault (Fig. 6).

Angular Unconformities In and Near the East Shoreline Fault Zone

Crosscutting relationships reveal progressive deformation of the Pleistocene to modern section in the ESF zone. The lower Brawley Formation is significantly more folded, faulted, and tilted than the overlying upper Brawley Formation in the ESF zone (Figs. 9 and 10; Markowski, 2016).

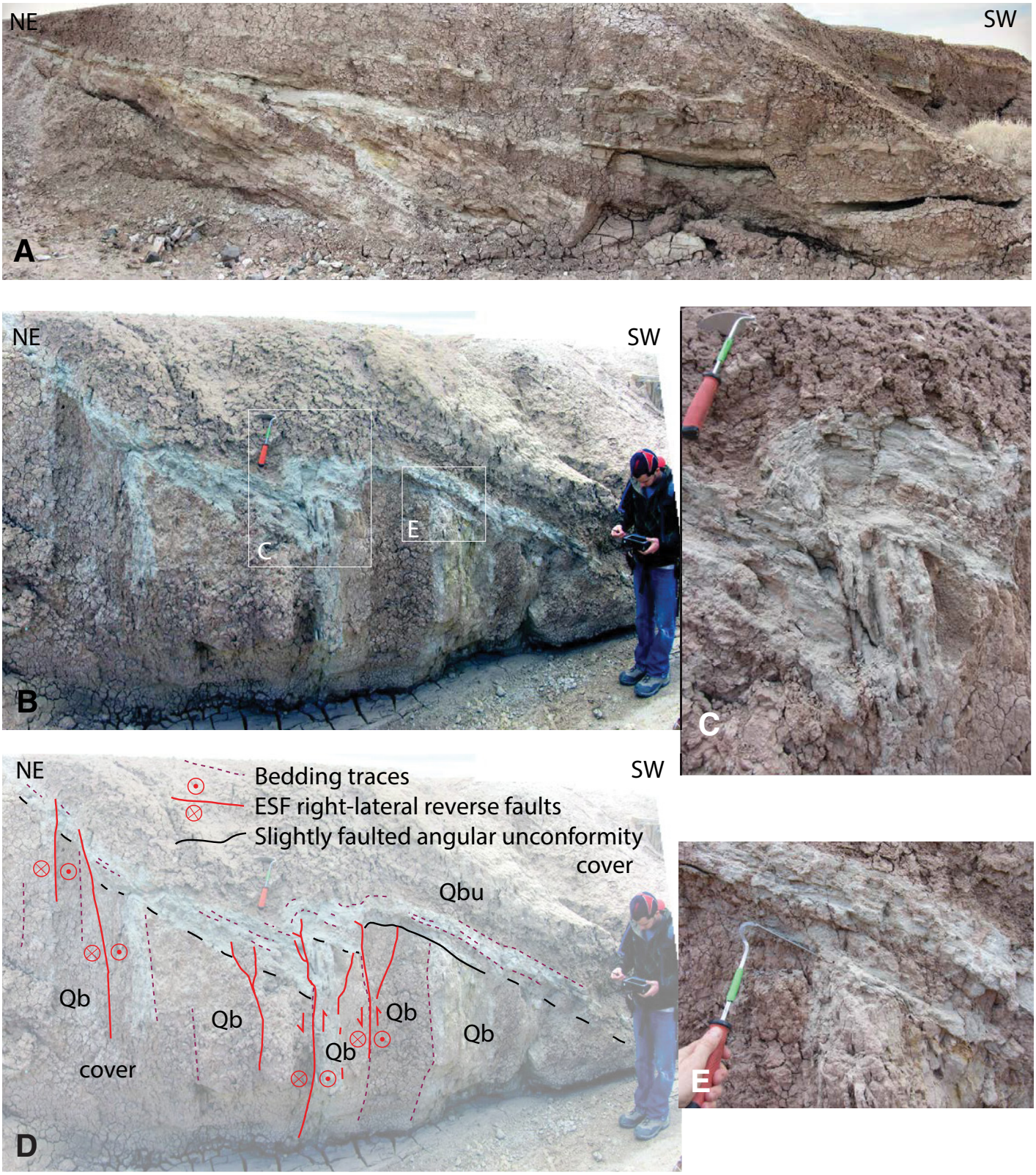

Figure 10. Annotated photographs of growth strata that preserve a faulted angular unconformity between the Upper Brawley Formation and Lower Brawley Formation. View is to the southeast. The upper scene (A) is 10s of meters basinward of the lowermost scenes (B to E). Notice that the faults in B and C are parallel to the steep Pleistocene beds and have flat-on-flat geometries below the unconformity. Mudstone is dark, and local-sourced fine sand and silt beds are white. The expanded views shown in C and E are marked with white boxes in B. See Figure 2 for the location near Bombay Beach, California. Qb—Lower Brawley Formation; Qbu—Upper Brawley Formation.

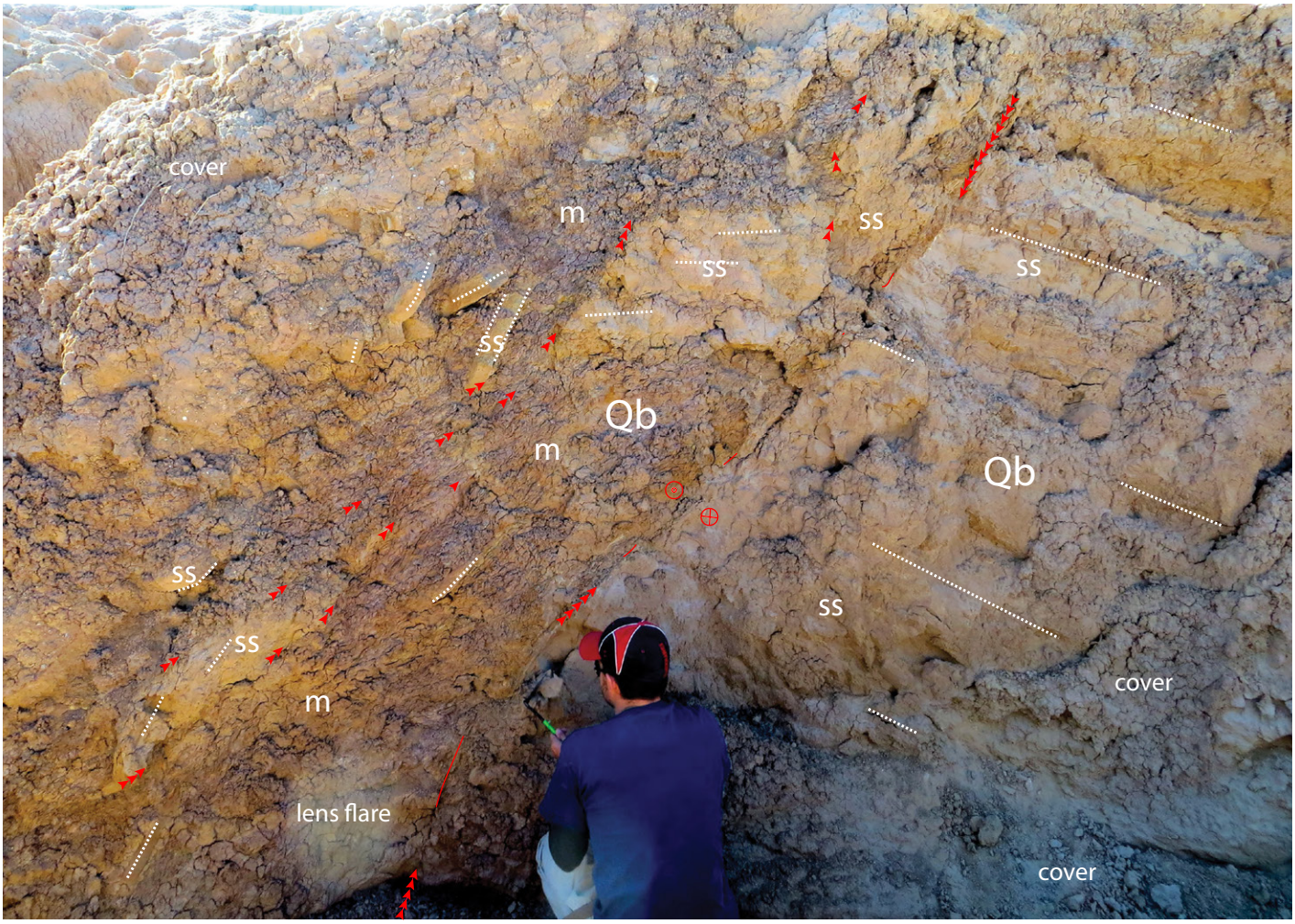

Figure 11. Annotated photograph of a right-lateral fault in the ESF of the Durmid ladder structure. View is to the northwest. There is a ramp in its footwall (right) and a disrupted flat in its hanging wall (left). The longest sequence of red arrowheads point to the main slip surface and fault core. Shorter red arrowheads point out a fraction of the faults in the damage zone. Note that the damage is localized in the mud-rich beds of the hanging wall of the fault. Mudstone (m) is redder and darker than the sandstone beds (ss) of the Brawley Formation (Qb).

Faulted modern and Holocene sediment within the fault zone are the least deformed, as expected (Fig. 9). Faults and folds deform all ages of rock and sediment in the ESF zone.

Angular unconformities in the upper part of the Brawley Formation (Fig. 4) are preferentially preserved in synclines of the ESF and adjacent parts of the Durmid ladder structure (Figs. 9 and 10; Markowski, 2016). Moderately to strongly tilted Brawley Formation beds are below the unconformity, and deformed, but noticeably less-tilted, less-folded, and less-faulted upper Brawley Formation beds lie above the unconformity (Figs. 9 and 10). The degree of differential tilting varies across individual angular unconformities, from one structure to the next, and records growth relationships within the ESF zone. Angular discordance of 50°–70° near several subvertical faults in the ESF zone give way a few hundred meters farther south to a discordance of 10°–20° across the same angular unconformity (Fig. 10). Pleistocene angular unconformities only occur within the younger parts of the Brawley Formation in Durmid Hill. These unconformities are probably younger than 0.5 Ma because they appear hundreds of meters up section from the 0.74 Ma Thermal Canyon Ash and the 0.76 Ma Bishop Ash (Fig. 4; Markowski, 2016). Localized deformation around each individual active fault zone explains this pattern.

A much younger set of angular unconformities formed between the deposits of the latest Holocene Lake Cahuilla, historic flood deposits from the 1905–1907 floods, overlying modern sediment, and all older units (Fig. 9). Those angular relationships are present throughout Durmid Hill. Lake Cahuilla postdated Holocene volcanism along the southern edge of the Salton Sea, and we used the presence of rounded pumice clasts from Upper Holocene volcanic centers (Schmitt et al., 2013) to distinguish between the richly fossiliferous and pumice-bearing Holocene sediment and the fossil-poor Brawley Formation.

Structural Evidence for the East Shoreline Fault Zone on Durmid Beach

The structures of the ESF zone continue unchanged onto Durmid Beach and the shallowest waters of the eastern Salton Sea (Fig. 12). Durmid Beach is a broad, 300–400-m-wide wave-cut platform with a thin and patchy carapace of beach sand and lagoonal mud. Folded and faulted Brawley Formation strata are exposed across much of Durmid

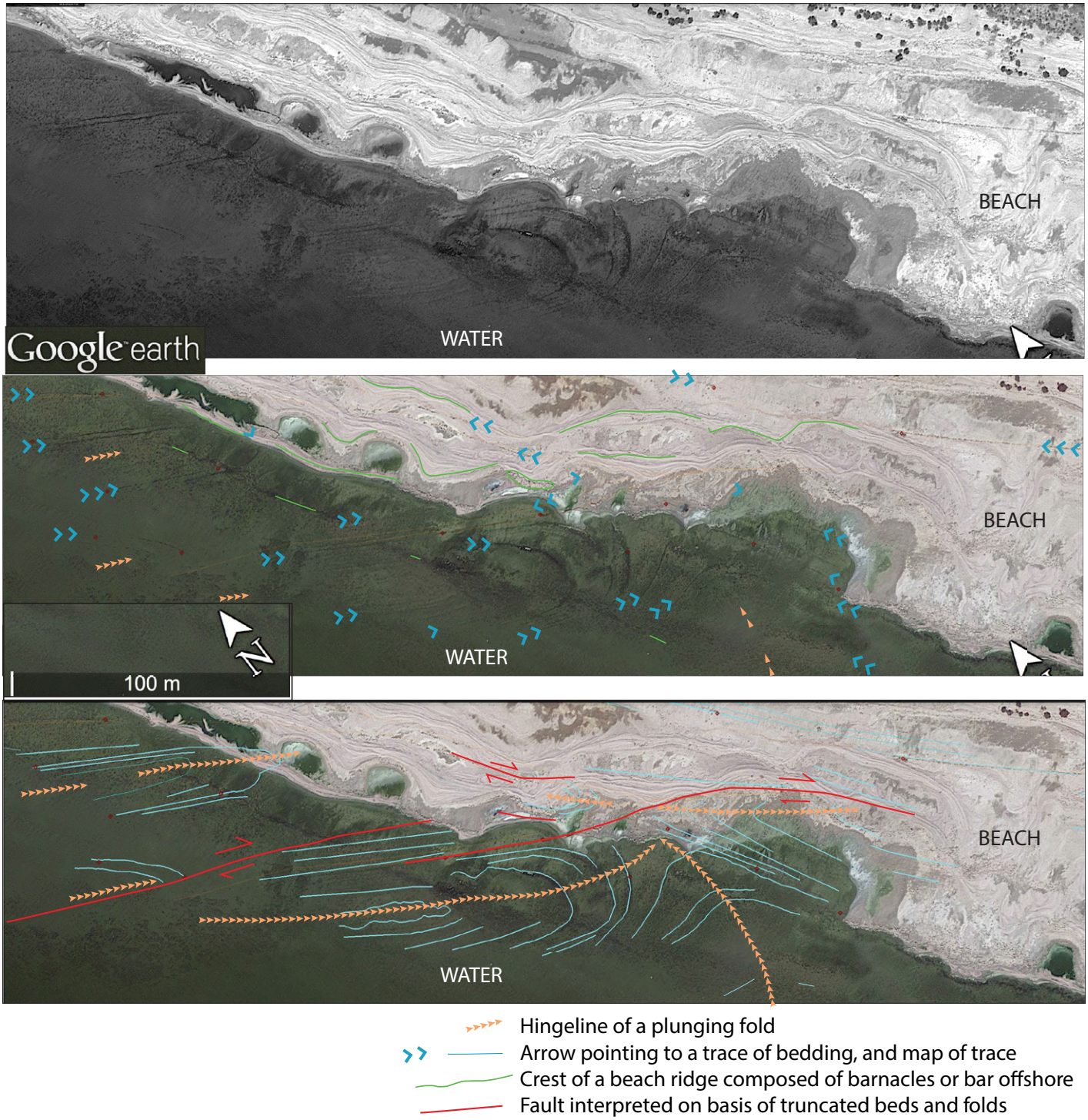

Figure 12. Annotated aerial image of the folded and faulted Brawley Formation exposed on the wave-cut terrace of Durmid beach in the ESF zone, in map view. Field work confirmed that the more resistant ridges on the beach are beds of the Brawley Formation. Hinges of plunging folds and bedding traces show that the northwest-trending structural fabrics of the transpressional ESF continue across the entire wave-cut platform and persist to at least 100 m offshore. Modern beach deposits are thin and mostly consist of wavy white beach ridges and intervening brown lagoonal mud. See Figure 2 for the location of this scene.

Beach below the modern lacustrine deposits. The northwest-trending structural geometries on Durmid Beach and in the shallow waters of the Salton Sea are identical to those on land in the ESF zone (Fig. 12). Many of the slightly raised linear ridges on Durmid Beach are cored by folded and faulted sandstone beds that are more resistant to erosion than the enclosing mudstone (Fig. 12).

A 1–2-m-high wave-cut escarpment separates the landward edge of Durmid Beach from the rest of Durmid Hill. The erosional escarpment and exposures of the Brawley Formation are less common between Salt Creek and the northeast corner of the Salton Sea than along the edge of Durmid Hill. The 1–2-m-high erosional escarpments like those along the northeast edge of Durmid and Corvina Beaches are unique along the perimeter of the Salton Sea and provide evidence of differential exhumation between the Salton Sea on its southwest side and exhuming Durmid Hill on its northeast side. The escarpments and depths of gullies show that the most-exhumed areas lie between Salt Creek area and Bombay Beach.

Imprint of East Shoreline Fault Zone and Durmid Ladder Structure on the Landscape

A comparison of the geologic map and digital elevation models reveals that the shapes of Durmid Hill and the Salton Sea are strongly controlled by the ESF zone, and to a lesser extent, by the mSAF (Fig. 3). The west slope of Durmid Hill is parallel to the folds, faults, and beds within the ESF zone (Figs. 2 and 3). The curvature of the steeper, easternmost floor of the Salton Sea closely parallels the curvature of the mapped faults, folds, and beds of the ESF zone from Bombay Beach in the south as far north as North Shore, California (Fig. 3).

The ESF probably persists southwest through some of the narrow band of steeper seafloor at the northeast edge of the northern Salton Sea. This band of steeper lake floor has the same slopes as the landscape of the subaerial part of the ESF nearby, and though gentle in an absolute sense, it is among the steepest lake floor around the Salton Sea (Fig. 3; Redlands Institute, 1999). The floor of the Salton Sea is remarkably flat. The seafloor and landscape in the ESF are linear to broadly curving in map view, except where the fan-delta of Salt Creek modified its shape. Other nearshore zones around the Salton Sea have more irregular shapes in map view than the part that coincides with the ESF (Fig. 3).

The distal southwest edge of the ESF is at most a few hundred meters offshore of Durmid Beach, in agreement with three reflection seismic lines that imaged features beneath the center of the Salton Sea (Sahakian et al., 2016). Those data document an unfaulted, ~10-km-wide block of gently northeast-tilted Quaternary sediments southwest of the Durmid ladder structure. The published reflection lines did not image the ESF (Sahakian et al., 2016).

The mSAF also controls the shape of Durmid Hill, but its relationship to topography is less consistent than that between the ESF and the landscape (red line in Fig. 3). From North Shore to south of Salt Creek, the mSAF is positioned along the southwest edge of a 300-m- to 1000-m-wide fault block of uplifted, internally folded and faulted Shavers Well and Brawley formations (Dibblee, 1954; Babcock, 1974; this study). This fault block forms a low ridge in the landscape for ~20 km, except where streams cut across it (Fig. 3). The ridge changes its geometry in the southern 5 km of Durmid Hill.

Deformation in Modern Sediment

Some faults of the ESF zone are well expressed, active, and marked by long, narrow, hairline right-lateral and secondary left-lateral fractures in all types of modern sediment along >18 km of the ESF zone. Most of the fractures occur in the western part of the fault zone on the upper half of Durmid Beach. All linear and continuous fractures coincide with fault zones when there is suitable exposure to allow the independent identification of fault zones. Secondary processes enlarged the original hairline microslips in a number of ways, and similar fractures and processes occur along the mSAF and some cross faults.

The mapped location, width, and shape of the ESF zone in Durmid Hill correspond closely with velocity fields in published interferometric synthetic aperture radar (InSAR) scenes of Lindsey et al. (2014) and Tong et al. (2013). Vertical velocity fields are particularly well correlated to the mapped geometry of the specific structure of the Durmid ladder structure (Janecke et al., 2016).

Southern Extent of the Durmid Ladder Structure

Mapping shows that surface traces of the ESF zone and the Durmid ladder structure pinch out and end at a branch point in shallow water southeast of Bombay Beach (Fig. 2). Mapped faults and folds in the ESF zone change strike progressively and curve eastward, parallel to the Salton Sea, as they approach Bombay Beach. Some faults strike 290° in this area, whereas 315° strikes dominate farther north. The clear imprint of the exhuming Durmid ladder structure on the landscape allows us to identify the southeasternmost extent of the ESF in the shallow water southeast of Bombay Beach (Fig. 3). The areas east of Bombay Beach expose widespread Holocene sediment, whereas inside the Durmid ladder structure, exhumation produces continuous exposure of Pleistocene Brawley Formation sediment (Fig. 2). The Salton Sea widens abruptly south of the southern tip of the SAFZ, by ~5 km on its east side, as plate motion shifted from the transpressional SAFZ to the BSZ in the south (Fig. 3).

Bombay Beach was built within the southernmost tip of the SAFZ, on exhuming Brawley Formation, yet the land on either side is buried beneath thick Holocene sediment. This latitude thus appears to lie simultaneously in the southern end of the Durmid ladder structure of the SAFZ and the northern extent of the BSZ (Figs. 1, 2, and 3). The transition zone between the SAFZ and the BSZ is partly on land and partly under the Salton Sea.

Structures Internal to the Durmid Ladder Structure

Cross Faults and Folds

The numerous west- and northwest-striking cross faults that connect the ESF zone across Durmid Hill to the mSAF together deform an uplifting damage zone of unusual width and organization within the Durmid ladder structure (Fig. 2; Janecke and Markowski, 2013a, 2013b, 2015a, 2015b; Janecke, 2013; Markowski, 2016). The left- and right-lateral cross faults that cut the rocks between the ESF zone and the mSAF in the study area vary in strike and often form fairly short bundles of strike-slip faults that branch, step, and die out into folds along strike (Fig. 2). A few groups of cross faults are arranged in en-echelon patterns, but most groups of faults have less-organized geometries.

Faults internal to the Durmid ladder structure are broad in map view, and many lack a fault core. We mapped those brittle fault zones as damage zones instead of faults (e.g., Fig. 5; Markowski, 2016). Discrete brittle faults deform the Pliocene to Pleistocene units at all scales, and this distributed brittle faulting mimics ductile shear (Figs. 5 and 13).

Strikes of cross faults and the intensity of deformation vary from one domain to the next. Groups of east-, southeast-, and east-southeast–striking, strike-slip cross faults connect to the master right-lateral faults of the mSAF across transitional zones where folds and faults bend toward parallelism with the master faults. Northeast-striking faults are uncommon in the Durmid ladder structure.

In the south, the largest concentrations of cross faults strike east- to east-southeast, have left separations, are vertical to steeply dipping, and consist of damage zones and discrete faults that generally have similar

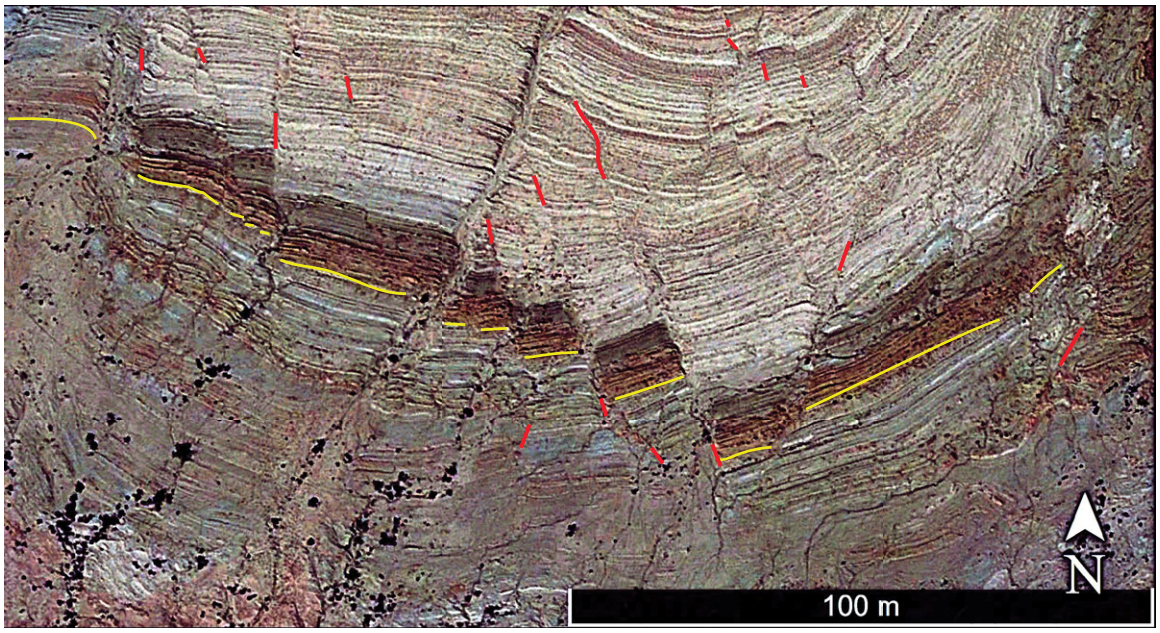

Figure 13. Annotated false color image of distributed faults (red) within the Durmid ladder structure. The yellow-brown marker beds of the Brawley Formation are displaced by many small right-lateral faults and a few left-lateral ones. Resistant beds in fault blocks superficially resemble boudins, but lack ductile thinning. See Figure 2 for location.

strikes as the well-known east-trending folds there (Figs. 2 and 5). Damage zones along cross faults range up to 70–90 m perpendicular to strike, but widths in the 5–30 m range are more common along cross faults. The spacing of the main zones of left-lateral cross faults is regular and about ~500–600 m, a distance that we will use later to estimate the amount of block rotation in this domain (Fig. 2). At their branch points with the master right-lateral faults, several cross faults change strike to more closely approach that of the mSAF and ESF, in the east and west, respectively (Fig. 2; Table 1; Markowski, 2016). Slip gradients along cross faults reflect the transfer of strain between faults and folds. Cross faults pervade the area and are more numerous than the folds (Figs. 2 and 5). Left-lateral separations range from ~650 m to ~1250 m.

In the north, approaching Salt Creek, cross faults strike northwest and cut highly disrupted and faulted sedimentary rocks, and there are many wavy lens-shaped fault blocks with northwest trends (Figs. 2, 6, and 14). Right-lateral cross faults form a denser and more anastomosing network of structures than the left-lateral cross faults, and they developed as multiple generations of crosscutting structures (Fig. 2). This northern area is so faulted and folded that the rocks there define a damage zone with block-in-matrix textures at the map scale. Its structural complexity makes it challenging to uniquely identify sedimentary formations or larger cross faults within this part of the study area.

Mapping on aerial and LiDAR imagery shows that cross faults are also present in the poorly exposed part of the SAFZ between Salt Creek and North Shore.

The Durmid ladder structure has many structural trends, yet there are few left- or left-normal faults that could be the onshore continuation of the north-northeast–striking Extra fault array (Figs. 1 and 2). However, those that exist are short and end at T-intersections with the more continuous right-lateral faults of the SAFZ. The lateral persistence of the ESF and its curving bathymetric expression suggest that the Extra fault array does not contact the mSAF, as was once thought or implied (Hudnut et al., 1989b; Lindvall et al., 1989; Brothers et al., 2011).

Comparison with Deformation East and West of the Durmid Ladder Structure

Rocks within the Durmid ladder structure are much more faulted and folded than the same-aged units on the east and west sides of the fault zone. West of the Durmid ladder structure, faults and folds do not deform the sediment beneath the northern Salton Sea, aside from subtle homoclinal tilting toward the ESF zone (Sahakian et al., 2016).

Field studies east of the Durmid ladder structure, in the Hidden Springs fault zone, revealed a modest amount of deformation that is notably less intense than that in the Durmid ladder structure. Left-lateral strike-slip faults in the Hidden Springs fault zone have northeast strikes, and the younger members of the Brawley Formation dominate the fault zone south of Salt Creek. By contrast, the highly deformed, folded and faulted areas within the Durmid ladder structure contain either east-striking, left-lateral strike-slip faults or right-lateral faults that are counterclockwise of the master mSAF and ESF zone.

The east strike of left-lateral strike-slip faults in the Durmid Hill area (Fig. 2) is unique in the northeast Salton Sea area, but such structures are common in ladder-like sections of the Coyote Creek and Clark faults on the southwest side of the Salton Sea (Kirby et al., 2007; Belgarde, 2007; Steely et al., 2009; Janecke et al., 2010a, 2010b; Thornock, 2013). This geometry is typical of domains that experienced differential block rotation in California (Dickinson, 1996). In order to produce the east strike of the left-lateral faults in the cross-fault domain of the Durmid structure, significant clockwise rotation is required (Markowski, 2016; see later herein).

Sense of Slip

Right-separations consistently are observed across northwest-striking steep faults of the Durmid ladder structure, and left-separations occur across east-striking subvertical faults and wide damage zones that define many of the fault zones in the cross-fault domain (Figs. 2, 5, and 14). These separations agree with the expected sense of slip for strike-slip faults and rotated strike-slip faults in the stress field of southern California.

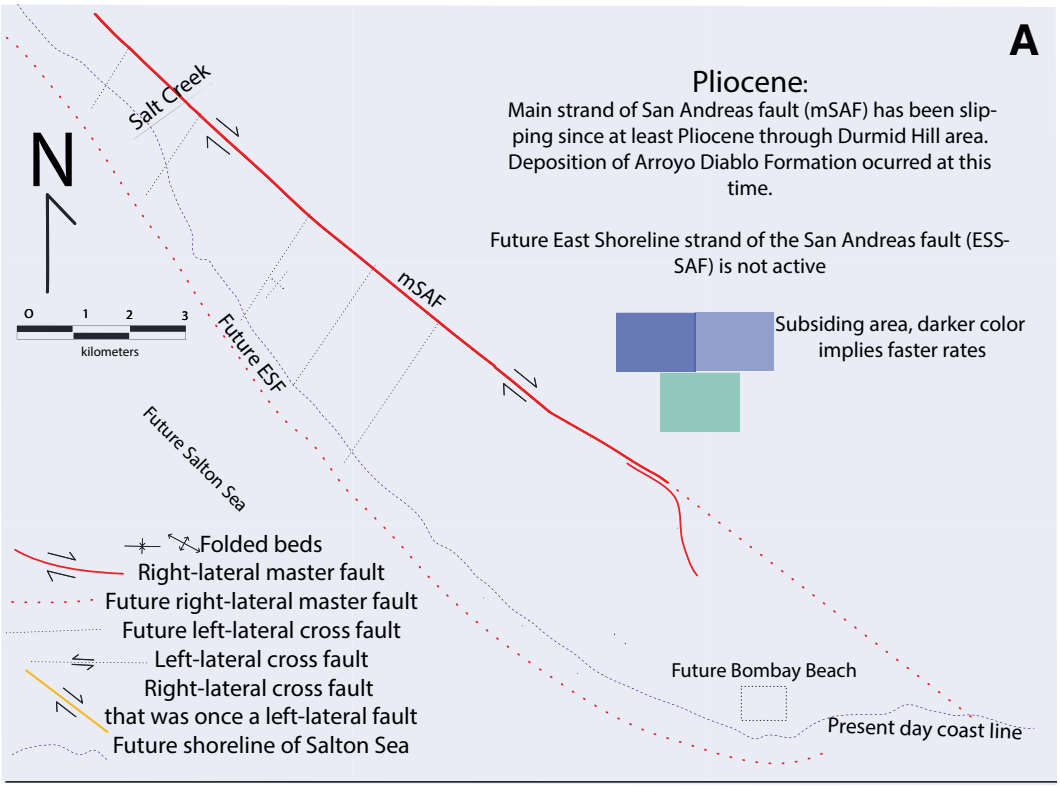

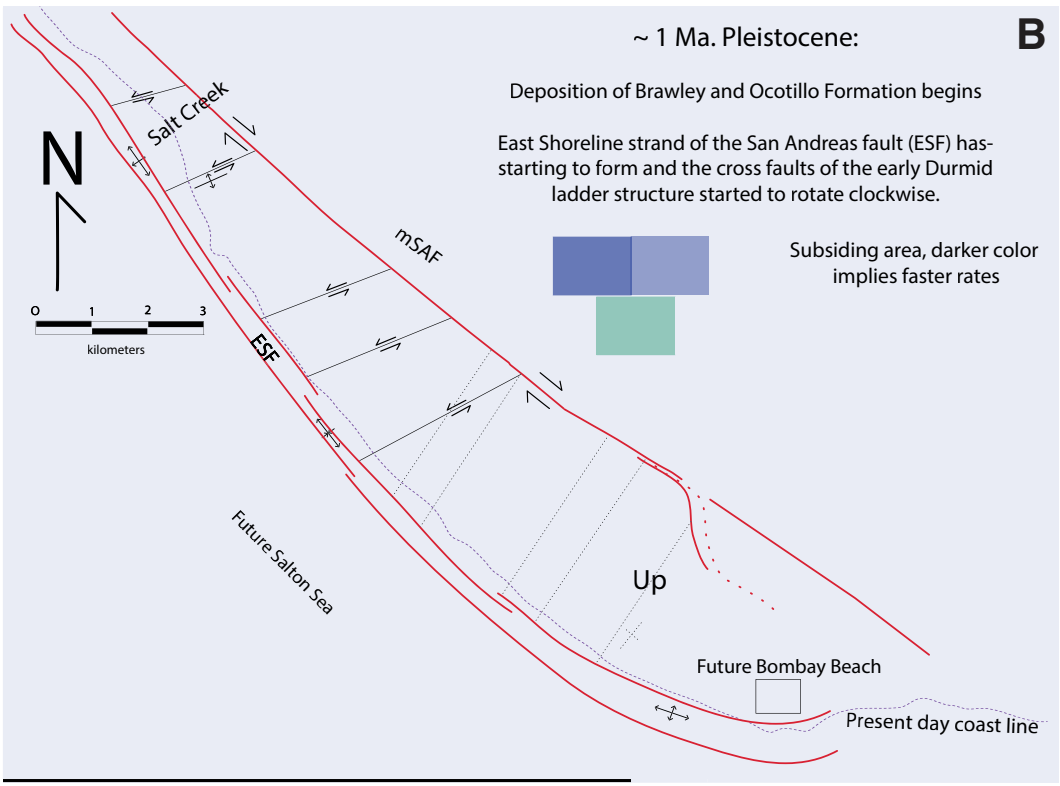

Figure 14. Diagram showing how the Durmid Hill ladder structure may have evolved. (A) About 6–4 Ma, the SAF has only one right-lateral strand in the Durmid Hill area. The fault core is fairly narrow, and it became more localized with time. (B) About 1–1.5 Ma Ma and before deposition of the Bishop Ash (~0.75 Ma), the ESF emerges and plate motion is now spread across the entire 3–4 km wide Durmid ladder structure. Left-lateral cross faults form and have northeast-strikes. There is regional subsidence and deposition of the lower Brawley Formation. (*Continued on following page.*)

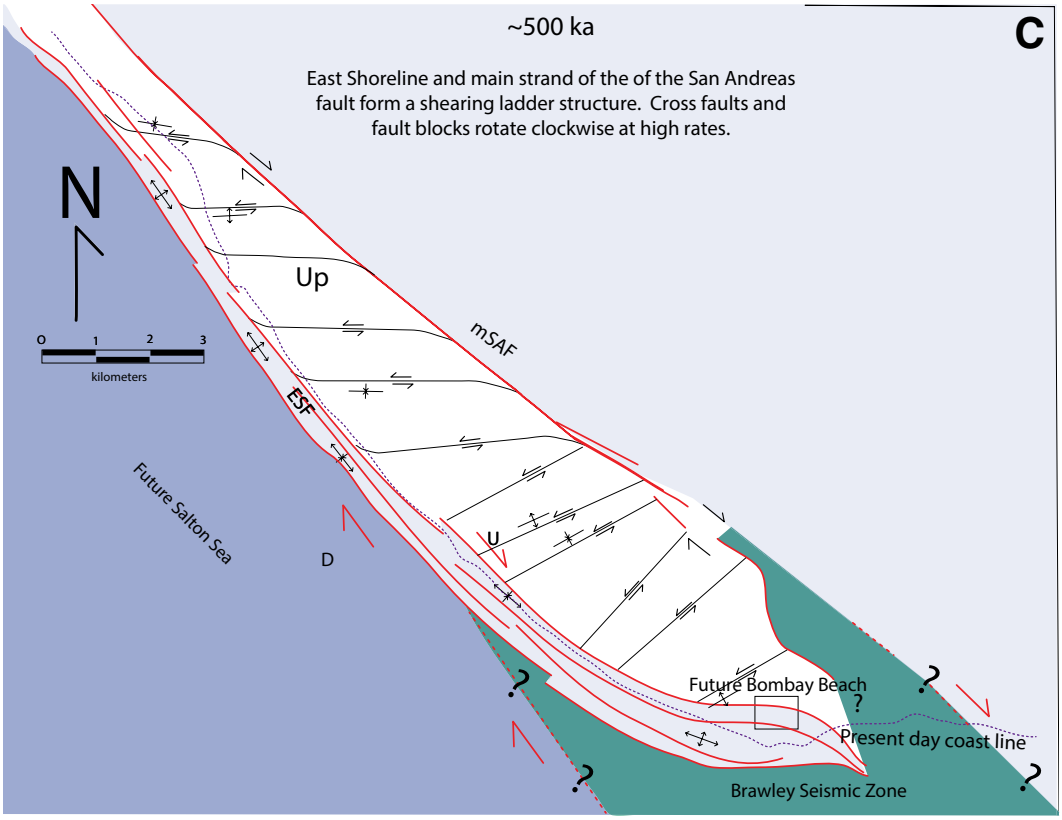

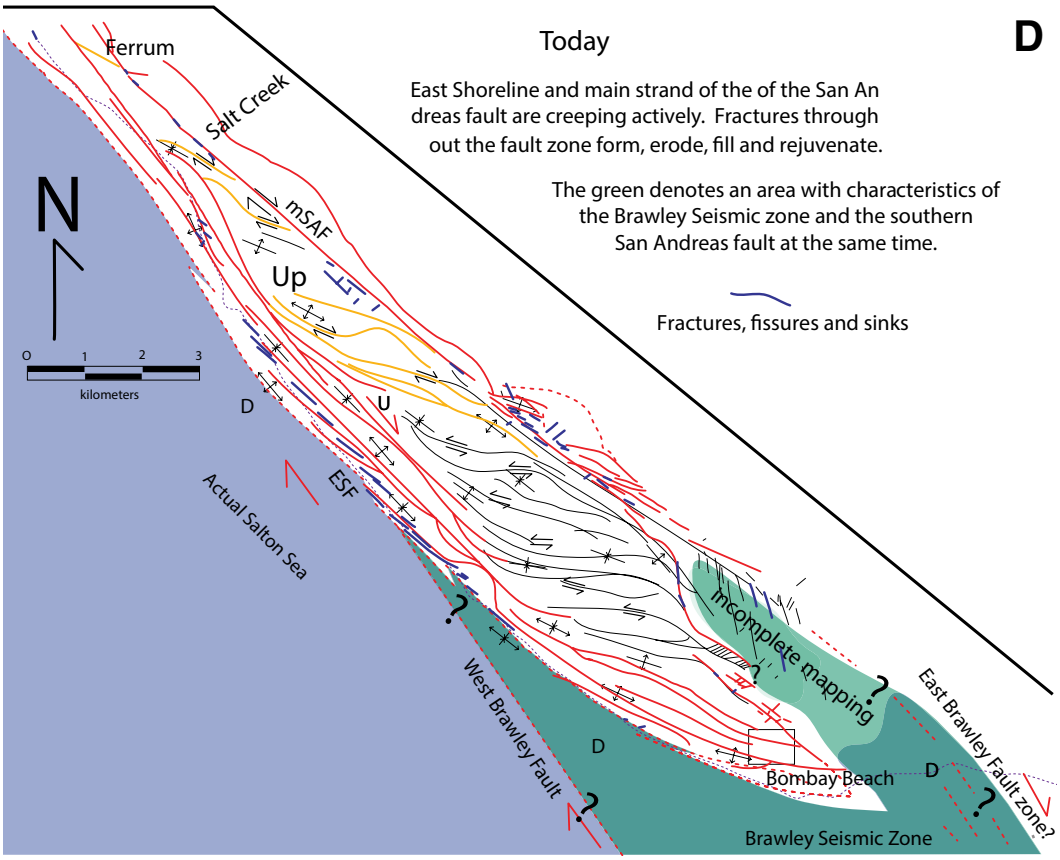

Figure 14 (*continued*). (C) The plate motion proceeds. Fault blocks rotate between the two master faults. The ESF becomes more complex, and more folds and right-lateral faults develop in its damage zone. Angular unconformities date from this time period, and there is differential uplift within and across the ladder structure. (D) The current condition. The ESF is so young that it is still a wide zone that lacks a fault core. The most active strands might be its southwest ones, beneath the shallowest edge of the Salton Sea. The southwest edge of the fault zone must lie east of the yellow squares in Figure 3. Fractures and evidence for creep (blue lines) occur on both edges of the Durmid ladder structure. The Brawley Seismic Zone and the northern Salton Sea are subsiding whereas the Durmid ladder structure is being exhumed and eroded. Our preliminary field studies suggest that the interaction between the SAFZ and the BSZ is taking place in the green triangles in C and D.

Slickenlines are not abundant on the fault surfaces in Durmid Hill, possibly due to the presence of substantial amounts of bedded gypsum in the stratigraphy. We have not been able to independently confirm the left-slip interpretation of east-striking faults and damage zones, but a different kinematic pattern is unlikely for faults with such geometries and separations embedded within the right-lateral San Andreas transform fault system.

Sigmoidal Map Pattern of Fold Axes and Fault Traces

We used quantitative structural analyses to examine the geometry of the folds in the southern two thirds of the study area, following Bürgmann (1991). Groups of complex folds commonly exhibit smaller parasitic and disharmonic attributes and are visible in map and cross-sectional views across Durmid Hill (Figs. 5, 7, and 12). We mapped them in detail in the southern Durmid Hill (Markowski, 2016). Farther north, near Salt Creek, the damage zones of the mSAF and ESF zone are so wide and nearly overlapping that the intervening domain of cross faults is less defined and contains mostly fragments of folds instead of mappable, laterally continuous structures (Fig. 2; Markowski, 2016). The significant faulting in the northern half of Durmid Hill precludes useful fold analysis there.

Map and cross-sectional patterns of bedding and fault traces on the gently sloping landscape along with fault orientations and our structural data sets reveal four structural fold domains in the southern two thirds of the area (Figs. 2, 3, 5, 7, and 8). We used an aggregate of the bedding orientations to determine the geometry of the typical fold axes in each domain (Fig. 2; Table 2). The 771 measurements of bedding constrain the fold forms in each domain.

The mean trend of folds nearest to the mSAF is 293°, and these folds plunge 9° to the west-northwest. This mean fold has an axis that is 15°–20° counterclockwise of the 311° strike of the mSAF (Fig. 2; Table 2). The east-west domain contains primarily east-west–striking, left-lateral strike-slip faults and folds that trend 284° and plunge 10° west. The transitional domain, even farther west, contains right-lateral and left-lateral strike-slip faults. The mean fold axis trends 295° and plunges 11° west-northwest in the transitional domain. This trend is ~17.5° counterclockwise from the average strike of the ESF zone (~312.5°).

The ~1–2-km-wide domain of folds in the East Shoreline domain is adjacent to the Salton Sea and contains primarily right-oblique, strike-slip faults, northwest-striking beds, and many folds (Fig. 12). The average fold trends 306° and plunges 1.4° north-northwest (Fig. 2; Table 2). The bedding orientations in this domain cluster into four subdomains that dip 31° and 54° northeast, and 29° and 62° southwest. These data show that folds in the ESF zone trend only ~5° and 6.5° counterclockwise of the strike of the mSAF, whereas folds closest to the mSAF are 18° counterclockwise of the master faults.

Bürgmann (1991) first identified this sigmoidal pattern of hinge lines from east to west across Durmid Hill. Our expanded analysis includes more measurements in the west, within the ESF zone, and that expansion reveals the greater amount of clockwise rotation of fold axes near the Salton Sea than near the mSAF. Folds in and near the ESF zone more closely match its strike than folds in and near the mSAF (Fig. 2; Table 2).

Faults internal to the Durmid ladder structure also have a sigmoidal map pattern (Fig. 2). In the cross-fault domain, faults strike east or west-northwest (Figs. 2 and 5). These nearly east-striking, left-lateral faults typically form wide and complex damage zones, and we were able to measure only a few attitudes of faults directly in outcrop. The adjacent domains contain mostly northwest-striking, right-lateral faults of the two strands of the SAFZ (Fig. 2).

Uplift and Shortening from Exhumed Formations

The oldest rock unit in the interior of the Durmid ladder structure is the Pliocene to Pleistocene(?) Arroyo Diablo Formation in the hinge zones of two large west-plunging faulted anticlines (Figs. 2 and 4; Markowski, 2016). These anticlines are shortening and uplifting in response to the strong transpression that pervades the Durmid ladder structure. The stratigraphic thickness of the overlying Brawley Formation indicates that at least 1.5–2 km of exhumation occurred to expose some hundreds of meters of the uppermost Arroyo Diablo Formation in these anticlines (Fig. 4).

The age of the Arroyo Diablo Formation is uncertain on the northeast side of the Salton Sea. Deposition of the Pliocene Arroyo Diablo Formation occurred between 4.8 and 2.2 Ma in its well-dated reference section in the Fish Creek Basin, which is currently ~60 km southwest (Dorsey et al., 2011). The absence of perennial lakebeds of the Upper Pliocene to Lower Pleistocene Borrego Formation in Durmid Hill, which normally separates the Arroyo Diablo Formation from the Brawley Formation (Dibblee, 1984; Kirby et al., 2007), implies that the Arroyo Diablo Formation northeast of the Salton Sea might be as young as early Pleistocene.

Leveling data, global positioning system (GPS) observations, InSAR data, and landscape features all show that that the entire Durmid ladder structure is uplifting (Babcock, 1974; Bilham and Williams, 1985; Sylvester et al., 1993; Lindsey et al., 2014; Markowski, 2016). Uplift is focused in the cross-fault domain, between the mSAF and ESF, but it also occurs within the damage zones of the two right-lateral strands of the SAFZ (Sylvester et al., 1993; Lindsey et al., 2014).

Our geologic map and previous results from gravity data further constrain the relative sense of vertical motion of basement across the mSAF in Durmid Hill (Fig. 3; Babcock, 1969, 1974; Langenheim et al., 2014). From northwest to southeast along Durmid Hill, a northeast-side-up component of motion across the mSAF in the Salt Creek area gives way a few kilometers to the southeast to a component of southwest-side-up motion (Fig. 3; Babcock, 1974; Langenheim et al., 2014). A ridge of shallow basement underlies the southern half of Durmid Hill between the ESF and mSAF according to the gravity data of Langenheim et al. (2014) and Figure 3. The uplift between the master faults of the southern Durmid ladder structure explains the presence of this ridge of high-density material at shallow depths, whereas prior interpretations of a single San Andreas fault trace do not.

A broad valley northeast of the Durmid ladder structure is underlain by the same Pliocene–Pleistocene formations as the Durmid ladder structure. The degree of deformation there is markedly less, however, and the upper Brawley Formation makes up a larger fraction of the exposed rock

TABLE 2. STRUCTURAL DATA FOR FOLDS IN FOUR DOMAINS OF THE DURMID LADDER STRUCTURE

Domain (from east to west)	Number of measurements	Mean dip of S or SW limb	Mean dip of N or NE limb	Orientation of the typical fold axis in this domain (trend/plunge)	Difference between trends of folds in this domain relative to those in the cross-fault domain	Difference between the trend of folds in this domain relative to the 311° strike of the main strand of the San Andreas fault (clockwise is positive)
1. San Andreas domain	149	58°	50°	293°/3.0°	9° clockwise	–18°
2. Cross-fault domain	209	50°	43°	284°/10°	N/A	–27°
3.Transitional domain	74	53°	49°	295°/11°	11° clockwise	–16°
4. East Shoreline domain	339	52°	47°	306°/1.4°	22° clockwise	–5°

(Babcock, 1974; this study). Broad expanses of Holocene lacustrine, eolian, and fluvial sediment in this broad valley indicate that exhumation northeast of the mSAF is slower than uplift in the ladder structure.

Changes as the Durmid Ladder Structure Approaches the Brawley Seismic Zone: A Preliminary Assessment

The southernmost SAFZ changes southward into a wide complex fault zone as it bends to a more northerly strike and interlaces with the northern end of the BSZ. The east and west edges of the BSZ are discrete faults in Imperial Valley, and we interpret a similar geometry beneath the Salton Sea in accord with prior work (Sharp, 1982; Fuis et al., 1982; Nicholson et al., 1986; Shearer et al., 2005; Lin, 2013; Hauksson et al., 2012, 2017). The boundary that separates seismically quiet or silent transpression of the SAFZ from seismically noisy transtension in the BSZ is abrupt and occurs at the shoreline of the Salton Sea directly east of Bombay Beach (Fig. 1; Hauksson et al., 2017). In contrast, the structural and landscape changes between the two fault zones appear to be spread across a fairly large volume of rock in southern Durmid Hill and the Salton Sea (Figs. 3 and 14).

The SAFZ widens southward from North Shore to Bombay Beach as it changes from the fairly narrow SAFZ of the Coachella Valley section into the Durmid ladder structure, and finally into the 4–10-km-wide BSZ (Fig. 1). In addition to widening toward the BSZ, the only part of the SAFZ in the Salton Trough known to contain numerous cross faults is the Durmid ladder structure, directly north of the BSZ.

The BSZ has many left-lateral cross faults between its bounding right-normal faults (see seismicity in Fig. 1; Fig. 3). These cross faults commonly activate during earthquakes swarms, and this provides much information about their location, geometry, and other properties at seismogenic depths (Shearer et al., 2005; Lin, 2013; Thornock, 2013; Hauksson et al., 2012, 2017). The geometries and seismic characteristics of the master right-normal fault zones are less clear, because moderate to small earthquakes have activated only a few of the right-lateral and right-normal faults of the BSZ (Figs. 1, 2, 3, and 14). This raises the possibility that the master right-normal faults preferentially rupture during large earthquakes, as they did during the 1940 Mw 6.9 and 1979 Mw 6.4 Imperial Valley earthquakes (Sharp et al., 1982; this study).

Due to a thick and pervasive Holocene cover and rapid subsidence, persistent seismicity beneath the lowlands of the southern Salton Sea and Imperial Valley, active source seismic studies, and gravity data provide much of what is known about the BSZ north of Mesquite Valley (Fuis et al., 1982; Shearer et al., 2005; Lin, 2013; Hauksson et al., 2012, 2017; Persaud et al., 2016; Han et al., 2016a, 2016b). The only faults mapped at the surface in the BSZ are in the south, along its eastern and western margins, and where they downdrop the Mesquite Basin as a transtensional graben relative to the rest of Imperial Valley (Sharp et al., 1982; Fuis et al., 1982). Those two bounding faults project northward along the outside edges of a north-northwest–trending cloud of small earthquakes (Fig. 1).

In contrast, the geometry of the many northeast- and north-trending cross faults within the BSZ is well characterized because they produce swarms of aligned earthquakes (Fig. 1; Johnson and Hadley, 1976; Fuis et al., 1982; Nicholson et al., 1986; Shearer et al., 2005; Lin, 2013; Hauksson et al., 2017). The northeast-striking faults produce mostly left-lateral focal mechanisms, and the north-striking ones produce normal focal mechanisms (Hauksson et al., 2017). In the north, near Bombay Beach, earthquakes disappear across a short lateral distance at the latitude where we identify the southernmost subaerial evidence for transpression and exhumation within the SAFZ. These data suggest that the northern end of the BSZ is immediately adjacent to the uplifting southern tip of the Durmid ladder structure, within a few kilometers of Bombay Beach (Figs. 1, 2, and 14).

Subsidence is a diagnostic feature of the BSZ, whereas uplift is a diagnostic feature of the SAFZ. A projection of the east and west margins of the well-located earthquakes of the BSZ north toward the Durmid ladder structure (Fig. 1) shows that there are two triangular areas on either side of the uplifting southern tip of the Durmid ladder structure that are intermediate in their elevation and structural style relative to the SAFZ and BSZ. These two triangular areas occupy a fairly low position in the landscape and widen southward, and the outer faults must curve, bend, or step somewhat to connect with the northward projections of the west and east BSZ faults. The inner faults of the two triangles, on the other hand, are strands of the SAFZ along the southern pinch-out of the Durmid ladder structure (Figs. 1, 2, 3, and 14).

The eastern triangular area is slightly above the Salton Sea, and some of it complex internal structure is exposed. Though mapping is ongoing, traverses show that this exhuming area is like the BSZ to the south, in that is has many small-displacement cross faults, numerous north-striking normal faults, thick deposits of Lake Cahuilla sediments, subsidence, and low topography (Fig. 3). Folded strata, however, resemble the SAFZ in the north. This on-land part of the transition zone between the SAFZ and BSZ spans ~6 km north to south. The western triangular area is hard to interpret because it lacks earthquakes, and it is beneath the Salton Sea.

Northern Extent of the East Shoreline Fault Zone and the Durmid Ladder Structure

We documented the ESF from Bombay Beach to the northeast corner of the Salton Sea through geologic mapping and landscape analysis (Figs. 1 and 3; Table 1; Markowski, 2016). From there northward, its location is less certain, and cross faults may no longer be present on its northeast side. Corvina Beach, about halfway between Salt Creek and North Shore, exposes the northernmost group of cross faults that we know of between the mSAF and the ESF zone. These cross faults are noteworthy because they damaged Highway 111 in more than six right-lateral zones. Each of the northwest-striking cross faults cuts the asphalt of Highway 111 in left-stepping and curving en-echelon fractures that have millimeter-scale right-lateral displacements from triggered slip or creep. The age of this deformation is not known.

Many lines of evidence suggest that the ESF zone and related structures probably continue northward for a considerable distance beyond the northeast corner of the Salton Sea (Fig. 1; Table 1). The uplifting young basin-fill deposits between the ESF and the mSAF are diagnostic of the paired strands of the SAFZ in a 30-km-long strip near the Salton Sea (red in Fig. 1), and we used this otherwise unexplained uplift to identify possible continuations of the ESF zone. We also explored the relationship between the Garnet Hill fault in northwest Coachella Valley and the ESF zone. Like the ESF zone, the Garnet Hill fault is partly responsible for uplifting large masses of basin fill between it and the Banning fault, the most active strand of the mSAF nearby (Fig. 1; Rogers, 1965).

The continuation of the ESF zone projects northwest along the edge of Coachella Valley and helps to explain an anomalous area of actively exhuming and uplifting basin fill on the southwest side of the mSAF in the western Mecca Hills (Fig. 1; Dibblee, 1954; Sylvester, 1988; McNabb et al., 2017). Between Box and Thermal Canyon, a 14 km by 1.5 km area of southwest-dipping Ocotillo and Upper Palm Spring Formations is exposed and being exhumed along the southwest side of the mSAF. Since almost every other mass of uplifted and eroding basin fill in the Salton Trough is being exhumed by active faults along their margins, we infer that the ESF is buried along the southwestern edge of the sedimentary rocks in the Mecca Hills.

The same argument suggests that the ESF may define the linear southwestern edge of a smaller block of exhuming Pleistocene conglomerate beneath Desert Park, northern Indio, California (Fig. 1; Rogers, 1965; Petra Geotechnical, Inc., 2009). Mapping, structural analysis, and drilling revealed a syncline that is parallel to the southwest edge of the uplifted fault block, and that rocks do not match across the southwest edge of the hill in the subsurface. This leads to the proposal of a northeast-dipping fault southwest of the Desert Park Hills that connects at depth with the mSAF (Petra Geotechnical, Inc., 2009). Faults and folds roughly parallel one another in the ESF zone near the Salton Sea, and a similar geometry may be present along the Desert Peak fault block.

Large blocks of uplifted basin-fill sediments on the southwest side of the mSAF are difficult to explain without the presence of a fault on their basinward margin. The ESF, subparallel to the strike of bedding and the syncline of the Desert Park area, could explain all the anomalous fault blocks (red overlay in Fig. 1). The distribution of uplifted basin fill along the margin of Coachella Valley also suggests a possible correlation between the ESF and the Garnet Hill fault, a short distance farther west-northwest (Fig. 1), because it also exhumes Pleistocene basin fill on its northeast side.

Additional corroborating evidence for a northward continuation of the ESF past the Mecca and Indio Hills emerges in migrated reverse-moveout reflections from lines 4 and 5 of the Salton Seismic Imaging Project across the Mecca and Indio Hills and Coachella Valley (Fuis et al., 2017; Hernandez et al., 2015; see Fig. 1 for locations). The most prominent package of reflections in line 4 through the Mecca Hills corresponds to the northeast-dipping surfaces of an unnamed buried fault zone that appears to be more clearly imaged than the nearby mSAF, which dips ~50°–60° northeast below a 6–9 km depth range, and more steeply at shallower depths (Fuis et al., 2017). The unnamed buried faults appear to be the along-strike continuation of the ESF zone, based on their location and geometric relationship with the mSAF (Fig. 1). The migrated reverse-move-out reflections from the SAFZ along line 4 reveal that the ESF may be the edge of a significant northeast-dipping flower structure (Fuis et al., 2017). In detail, the reflection data suggest that the ESF zone may be antilistric near the surface and listric at greater depth where it merges with the mSAF (Fig. 15; Fuis et al., 2017).

Migrated reverse-moveout reflections from SSIP line 5 across the Indio Hills in northern Coachella Valley similarly image 4–6 moderately to steeply northeast-dipping reflections in a zone 3–5 km southwest of the Banning fault. The Banning fault is the mSAF at this latitude, and it is the most prominent reflector in the migrated data set. Its reflections persist from the surface to ~4 km depth with no obvious dip change. The many reflections to the southwest of the Banning fault are probably the northwestern continuation of the ESF zone and the southeastern continuation of the Garnet Hills fault, where they may step left, bend, or step and bend toward one another (Hernandez et al., 2015). The dip directions of the SAFZ in lines 4 and 5 are similar, and northeastward, but there is less evidence for downward convergence or flower structures along line 5, although this type of feature is not excluded (Hernandez et al., 2015). Along lines 4 and 5, the ESF zone and the Garnet Hill fault are the only known faults that could produce the strong reflections southwest of the mSAF zone.

Groundwater chemistry patterns may also show the presence of a fault. Groundwater sodium sulfate concentrations exhibit a sharp linear boundary with calcium-bicarbonate–bearing waters of the adjacent aquifer (blue line in Fig. 1; Robbins and Reyes, 2012). The boundary coincides with the projection of the Garnet Hills fault (Robbins and Reyes, 2012) and with the southwest edge of a packet of reflections on line 5 (Hernandez et al., 2015). Correlation of the ESF zone with the Garnet Hills fault could explain these observations.

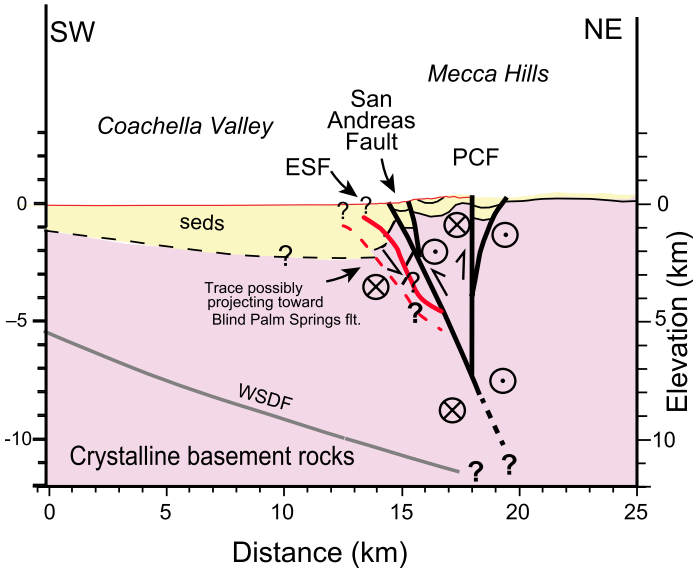

Figure 15. Interpreted cross section through the ESF and mSAF in the Mecca Hills in southern Coachella Valley. Modified from Dorsey and Langenheim (2015) and Sahakian et al. (2016) to include northeast-dipping traces of the ESF that Fuis et al. (2017) imaged seismically in Line 4 along the southwest edge of a San Andreas-centered flower structure in the Mecca Hills. The solid red trace of the ESF in the Mecca Hills is more continuous and reflective than the dashed trace. We infer similar relationships beneath Durmid Hill except that there must be much additional complexity due to numerous cross faults. Maximum thickness of the basin fill was reduced from 5 km to 3 km to honor the new data of Fuis et al. (2017) and Sahakian et al. (2016) about the depth to higher velocity materials. ESF—East Shoreline fault; WSDF—West Salton detachment fault; PCF—Painted Canyon fault; SSAF—Southern San Andreas fault. See Figure 1 for locations of the cross section and line 4.

Holocene to latest Pleistocene beds in Coachella Valley and the Salton Sea dip uniformly toward the SAFZ and have slightly steeper dips at depth than in the shallowest crust due to progressive deformation (Dorsey and Langenheim, 2015; Hernandez et al., 2015; Sahakian et al., 2016; Fuis et al., 2017). The mSAF was thought to be the northeast margin of this regional tilted block (Dorsey and Langenheim, 2015,) but that is not possible because southwest-dipping sedimentary rocks dominate each of the northern three red fault blocks of Figure 1 (Sylvester and Smith, 1976; Dibblee, 1997; Petra Geoscience Inc., 2009). A major structure like the ESF zone must separate the southwest-dipping sedimentary rocks in each fault block from the younger sediment in the northeast-tilting Coachella Valley block (Fig. 15).

Altogether, the nature and presence of exhuming basin-fill deposits, strong steep reflections in two seismic lines, tilted blocks, southwest dips of sedimentary rocks southwest of the mSAF, synclines, and the chemistry of groundwater suggest that the ESF zone persists along the entire northeast margin of Coachella Valley. If the ESF zone becomes narrower in the north, it could step left to the Garnet Hill fault, or bend to become the same structure (Table 1). The northward continuation of the ESF zone bends along strike, roughly parallels the mSAF, and lies 1–4 km southwest of the mSAF.

We also explored the possibility that the ESF branches northward, because the SAFZ in the Salton Trough has many such branches on its northeast side (Fig. 1). Northward-diverging branches far out-number southward-diverging ones along the Coachella section of the SAFZ.

DISCUSSION AND ANALYSIS

Great Width of the SAFZ in the Durmid Ladder Structure

The damage zone and the surface expression of the southernmost SAFZ are much wider and much more complex than previously inferred along its southernmost trace. Our results show that the right-lateral Durmid ladder structure is the primary expression of the southern SAFZ, and it has a ladder-like geometry all along the margin of the northern Salton Sea (Figs. 1 and 2). The mSAF and ESF zone are part of a coordinated sheared ladder-like fault zone in map view, and they bound dozens of left- and right-lateral cross faults and folds between them. Contrary to traditional interpretations of strike-slip faults as relatively narrow vertical planes, the Durmid ladder structure deforms a large volume of rock. At its widest, the elongate lens-shaped Durmid ladder structure might be as much ~4–5 km wide at the surface, depending on whether we include the incompletely understood damaged rocks on the northeast side of the mSAF. This width probably persists to a depth of several kilometers (Fuis et al., 2017). Ladder-like fault zones occur at all crustal levels and form in sedimentary rocks as well as crystalline rocks (Shearer et al., 2005; Lin, 2013; Sharp, 1967; Ross et al., 2017). Many large earthquakes have ruptured through broad strike-slip fault zones that have ladder-like components (Kroll et al., 2013; Milliner et al., 2015; Clark et al., 2017).

Northward, the Durmid ladder structure narrows to 1–1.5 km perpendicular to strike. Since the inclusion of fault zone plasticity greatly reduces the maximum predicted ground shaking of a large earthquake along the SAFZ (Roten et al., 2014), a kilometer-wide fault-and-damage zone of a ladder-like fault zone may significantly dampen ground-shaking and directivity effects.

Transpression in the San Andreas Fault Zone

Evidence for contraction, uplift, and exhumation is pervasive in the Durmid Hill ladder structure. Folds and steep Pleistocene beds are the most prominent indicators of transpression in the Durmid Hill area, and they are ubiquitous in all parts of the structure (Figs. 2, 9, and 10; see also Babcock, 1974; Bürgmann, 1991). The growth relationships within the Brawley Formation and beneath the deposits of Lake Cahuilla indicate that the Durmid ladder structure was active during deposition of these units. Folds record the overall contractional component of deformation across this section of the SAFZ, and these transpressive structures are the result of the well-known counterclockwise orientation of the mSAF along Durmid Hill relative to more northerly plate-motion vectors (Bilham and Williams, 1985). The Durmid ladder structure is thus part of a contractional bend along the SAFZ. Uplift and incision throughout the Durmid ladder structure are evidence of strong transpression.

Transpression within the ESF zone is easier to recognize than within the damage zone of the mSAF due to the smaller amounts of total shearing, and the more intact rock units, but strong shortening is present throughout the Durmid ladder structure, and normal faults are rare in the SAFZ. Shortening is fairly uniformly recorded in the ~1-km-wide ESF zone and evidenced by the mapped fault-fold pairs throughout this structure (Figs. 2, 7, 8, 9, 10, and 12).

Compelling evidence that the mSAF dips northeast throughout Coachella Valley and east of the Salton Sea includes aligned earthquakes, analyses of seismic refraction and reflection and gravity data, and geologic relationships (Lin et al., 2007; Fattaruso et al., 2014; Fuis et al., 2012, 2017; Markowski, 2016; Dorsey and Langenheim, 2015; this study). The evidence for pervasive contraction in the rocks of the ESF zone contradicts a transtensional interpretation of seismically imaged beds with a faint fanning geometry beneath the Salton Sea, west of Durmid Hill (Sahakian et al., 2016). Our data agree with prior well-documented evidence for a Quaternary transpressional strain field along the SAFZ near the Salton Sea (Babcock, 1974; Bilham and Williams, 1985; Bürgmann, 1991). Further, Dorsey and Langenheim (2015) and Fuis et al. (2012, 2017) showed that the northeast dip of basin fill southwest of the San Andreas fault is due to footwall deformation beneath the northeast-dipping, right-reverse SAFZ, of which the Durmid ladder structure is an integral part (Fig. 15).

The interpretation of velocity data in line 7 by Sahakian et al. (2016) is at odds with the bulk of the evidence presented here and with data and interpretations of Brothers et al. (2009, 2011) and Sahakian et al. (2013, 2014). Line 7 crosses a narrow part of the Durmid ladder structure north of Salt Creek and continues under the Salton Sea, where it is interpreted to show a single, southwest-dipping, listric transtensional fault that projects to the surface at the ESF. The "listric" boundary, with the most rapid lateral changes in velocity (the inferred fault zone), projects to the surface on the wrong side of the San Andreas fault (northeast instead of southwest side) and dips northeast instead of southwest where it is imaged in line 16 of Kell (2014) and Sahakian (2015).

We suggest an alternative interpretation of line 7 that explains the curved top of higher-velocity rocks imaged by Sahakian et al. (2016) as a composite feature formed by right-reverse deformation distributed across the 7–10 faults in the profile (Figs. 1, 2, 3, and 15). Sahakian et al. (2016) considered only two of these faults in their interpretation. From northeast to southwest, the 7–10 right-lateral and right-reverse faults are the Powerline, East and West Hidden Springs, several traces in the Bat Caves Butte fault zone, the mSAF, cross faults, and several faults within the ESF zone (S. Jänecke, D. Markowski, and J. Evans, unpublished mapping, 2012–2018). Progressive northeast-side-up vertical components of deformation across most of these faults produced a faulted basement-cover contact that superficially has a curving "listric" geometry in the velocity profile of line 7 (Fig. 15). Gravity data, migrated reverse-moveout reflections from seismic line 4 across the Mecca Hills in Coachella Valley, and sparse earthquakes downdip of the SAFZ are consistent with our interpretation of the ESF zone and Durmid ladder structure as a northeast-dipping zone of faults (Figs. 3 and 15; Lin et al., 2007; Lin, 2013; Fuis et al., 2012, 2017; Langenheim et al., 2014).

Rotation Rates Within the Ladder Structure

The overall geometry of the Durmid ladder structure and the easterly strike of the left-lateral cross faults between the ESF zone and the mSAF in the southern Durmid Hill area imply that large amounts of block rotation have occurred and that rotation is likely ongoing (Fig. 16). There are two ways to estimate the amount of block rotation. The simplest method compares the current strike of the left-lateral strike-slip faults in the ladder structure with their ideal geometries in the regional stress field. The stress field of southern California nominally should produce northeast- to east-northeast–striking, left-lateral faults, which implies that ~45° of clockwise rotation has occurred.

A second, more specific reconstruction builds on the analysis of Dickinson (1996). We created a physical block model with length scales that match those in the southern cross-fault domain in Durmid Hill. We affixed a cut-up version of the geologic map in Figure 2 to movable fault blocks and restored the offset markers in southern Durmid Hill by back-slip across left-lateral faults and concurrent block rotation. The left-lateral fault zones are spaced 500–600 m apart and have left separations between ~550 and 1250 m (see above and Fig. 2). Clockwise rotation of 45° produced only 500–600 m of left-lateral slip, and the block model showed that 55°

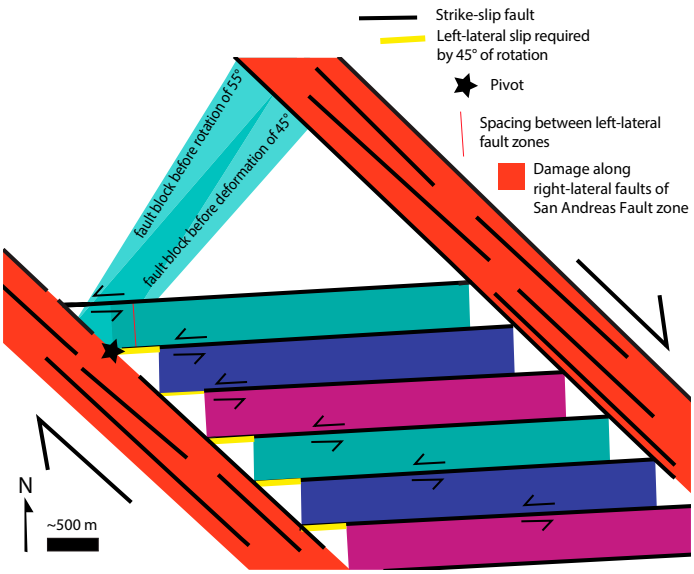

Figure 16. Simplified sketch of a physical block model that we created to relate left-lateral slip to block rotation. Fault-bounded blocks within this ladder structure have the length scales that match east-striking cross-faults in southern Durmid Hill (Fig. 2A). The current geometry is depicted with opaque colors, and adjacent blocks of rock have unique colors for clarity. Two possible restored geometries of the uppermost fault block are shown with a transparency. The uppermost teal fault-block must have rotated roughly 55° clockwise to restore the left-lateral separation of numerous mapped marker beds in the Brawley Formation (Fig. 4; Markowski, 2016). The blue bed in Figure 5, for example, was displaced almost 1 km. A simple rule of thumb is shown: The spacing between cross faults equals the left-slip across them, when 45° of clockwise block rotation has accrued. See the text for more discussion.

± 5° of clockwise rotation was needed to restore the marker beds in the geologic map (Figs. 2 and 16).

Altogether, many east-striking, left-lateral strike-slip faults between the ESF zone and the mSAF appear to have rotated as much as 45°–60° clockwise between the two right-lateral strands of the San Andreas fault since their inception in the Pleistocene. Conjugate, left-lateral faults outside the Durmid ladder structure do not show evidence of such large rotations. The left-lateral strike-slip faults northeast of the ladder structure in the Hidden Springs fault zone strike northeast, as do those in the Extra fault zone southwest of the structure (Brothers et al., 2009; Thornock, 2013). This geometry of left-lateral faults is expected in the regional stress field of southern California (Yang and Hauksson, 2013). The different strikes of left-lateral strike-slip faults in the Durmid ladder structure relative to those outside of the structure reflect much less or no rotation outside of the Durmid ladder structure than within it.

There is much more stratal disruption and shear across the domain of right-lateral cross faults in the cross-fault domain of northern Durmid Hill than in the domain of left-lateral cross faults in the southern half of Durmid Hill. The northern half of Durmid Hill is also narrower than the southern half. These patterns suggest that the right-lateral cross faults of northern Durmid Hill probably slipped more than the domain of east-striking left-lateral faults in the south (Fig. 2). If so, the northern cross faults may be older than the southern group and may have initiated as northeast-striking, left-lateral faults prior to large clockwise rotations that transformed them into right-lateral faults. Figure 14 depicts this possibility.

If our hypothesis is correct, block rotation progressed enough within the sheared ladder-like fault zone to cause reversals of the sense of slip across some strike-slip faults, from their original left-lateral sense to their current right-lateral displacements (Fig. 14). Testing our interpretation with paleomagnetism is not likely to be fruitful because the rocks of Durmid Hill are remagnetized (Strauss, 2011) and strongly deformed.

An unexpected implication of large clockwise rotation in the cross-fault domain is that the nearly east-trending folds that grossly parallel the left-lateral strike-slip faults of southern Durmid Hill (Fig. 2) cannot be the result of wrench processes, because wrench folds form oblique to left-lateral strike-slip faults instead of having trends that almost parallel them (Fig. 2D). We conclude that the folds must have originated with northeast trends and then were rotated to their present orientation (Fig. 14).

Other Ladder-Like Fault Zones

The BSZ is a transtensional structure that strikes 335°–340° and subsides between its eastern and western bounding fault zones (Fuis et al., 1982; see also Fig. 1), in contrast to the uplifting and transpressional Durmid ladder structure (Sylvester et al., 1993; Lindsey et al., 2014; Markowski, 2016; this paper). The ladder-like geometric relationships between right-lateral master faults and left-lateral rung faults of the BSZ are recognized through its aligned microseismic events and swarms (Johnson and Hadley, 1976; Nicholson et al., 1986; Shearer et al., 2005). These swarms delineate mostly cross faults and a small fraction of master right-lateral-normal faults (Magistrale, 2002; Shearer et al., 2005; Lin et al., 2007; Thornock, 2013; Lin, 2013). Current microseismicity and earthquake swarms preferentially activate the rungs of the BSZ, and many large earthquakes have ruptured through broad strike-slip fault zones that have ladder-like components (Kroll et al., 2013; Milliner et al., 2015; Clark et al., 2017). It is possible that future major earthquakes may localize along the seismically quiet master faults of the BSZ in the future.

The ~310°–315° strike of the ladder-like zone in Durmid Hill is ~20°–30° counterclockwise of the overall trend of the BSZ, and this strike explains its strongly transpressional nature (Bilham and Williams, 1985). The southern end of the SAFZ resembles the BSZ more than it resembles the SAFZ farther north because it has a ladder-like geometry in map view and gradually widens to match the ~6-km-wide BSZ directly to the south.

Durmid Ladder-Like Fault Zone and Its Role in Forming Damage Zones at All Scales

The width and geometry of fault and damage zones in the Durmid Hill area have implications for understanding earthquake processes. The many scales of damage in the Durmid ladder structure show how complex and variable damage can be. The entire Durmid ladder structure can be treated as a single damage zone when viewed at the scale of the Salton Trough and the Salton Sea (Fig. 17). Closer in, map-scale damage occurs along each of the master right-lateral faults and along each of the larger cross faults (Figs. 5 and 6). Some fault strands within the Durmid ladder structure are themselves smaller ladder structures defined by master faults a few tens to a few hundreds of meters apart.

At the next closer scale of observation, across <50 m perpendicular to the strike of a fault-fold pair, damage zones lie along the medium-scale faults. Individual exposures of fault zones at the outcrop scale commonly exhibit damage zones that are tens of centimeters to several meters thick perpendicular to the central strike-slip fault (Figs. 8A, 8B, 11, and 17).

The intersection of the master right-lateral strands of the San Andreas fault and the cross faults appears to explain the highly asymmetric position of the most faulted and folded damage zone southwest of the mSAF

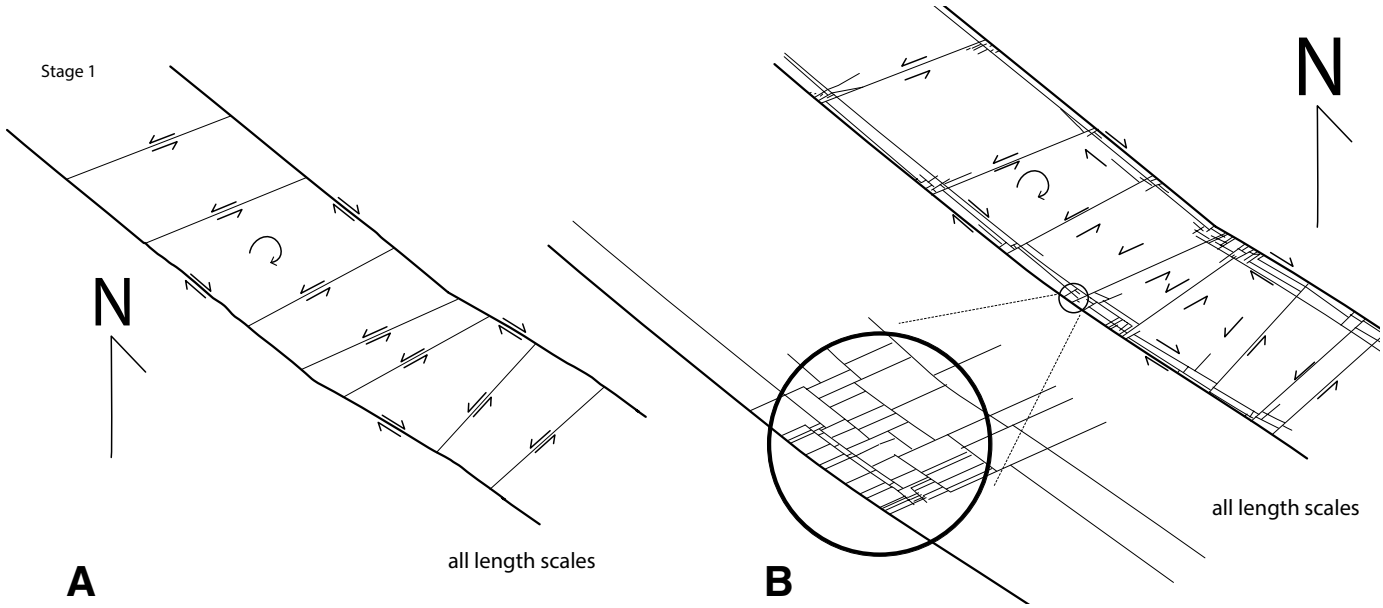

Figure 17. Schematic drawing illustrating the process that may explain the highly asymmetric damage zone that is localized on the inside of the Durmid ladder structure (Fig. 2A). We infer that the fault core and main slip surface of the master right-lateral faults will localize on the smoother, less disrupted outside edges of the ladder structure over time as its more interior traces become disconnected by slip on the cross faults within the ladder structure.

(Fig. 17). By activating both right-lateral master faults and cross faults at high angles, the mutual interference between them produces highly faulted rocks on the inside of any ladder-like fault zone. The outermost right-lateral master faults (the mSAF and a submerged strand of the ESF in this case) are not cut in the process, and they can continue to slip smoothly past the developing damage zone on the inside of each master fault.

How Might Earthquakes Interact with the Durmid-Brawley Fault Zone?

Several processes could trigger a northward-propagating unilateral rupture along the southern SAFZ or BSZ. Left-lateral or left-normal slip on a strike-slip fault southwest of the SAFZ is one possibility (Hudnut et al., 1989b; Brothers et al., 2009, 2011). To date, analysis has focused entirely on the Extra fault array as possibly triggering such an event because it is the only left-lateral fault zone thought to intersect with the southern SAFZ in the Salton Trough. The revised structural geometry of the SAFZ and BSZ documented here suggests that the numerous left-lateral faults west of the BSZ may also trigger earthquakes that rupture northward onto the Durmid ladder structure and onto the SAFZ farther north. Triggering by left-slip on faults west of the SAFZ and BSZ (such as the Elmore Ranch and Westmoreland fault zones; see Fig. 1) is kinematically more likely to activate the western parts of the Durmid ladder structure and the master faults in the western BSZ. Intersecting active faults on the North American side of the plate boundary with right-lateral components of deformation could activate northward-propagating earthquakes in the eastern edges of the two ladder structures. Faults like the right-normal Hidden Springs fault zone may be capable of triggering large events along the mSAF and east Brawley fault zones.

Rockwell et al. (2011) and Meltzner et al. (2016) showed that the BSZ and San Andreas fault in Coachella Valley may have ruptured simultaneously during one or more past earthquakes. Their hypothesis is consistent with our preliminary demonstration of the gradational structures in the boundary region between the SAFZ and the BSZ. Together, their results and ours imply that some major ruptures along the southern SAFZ could originate within the BSZ and propagate northward toward the more densely populated parts of southern California.

Zoning and hazard analysis do not typically consider fault zones as wide as the Durmid ladder structure when planning for their potential impact on communities and lifelines. Many metropolitan areas in strike-slip–faulted regions lie in basins composed of layered rocks like those in the Salton Trough, and similar structural styles of faulting may be present there. It would therefore be wise to explore the trade-off between a much wider potential footprint of surface faulting in active ladder structures and the smaller surface displacements that might occur across each individual fault traces in the larger array. Significant errors might be introduced if active faults are represented as simple surfaces and lines on Earth's surface rather than as fault zones (Bryant and Hart, 2007; Fletcher et al., 2014).

Neutral to mildly extensional zones farther north along the San Andreas fault or to the south in the BSZ may be more likely to nucleate future large earthquakes than the southern tip of the fault zone. An earthquake on any active right-lateral fault on the northeast side of the SAFZ–BSZ could modulate stresses across the broad SAFZ–BSZ band and trigger a northward-propagating rupture. Many such faults have been mapped in the region (Fig. 2).

Recognition of a different structural geometry along the southern SAFZ has many implications for hazards and for understanding many processes of earthquake rupture. Relative motion has been distributed across this entire ladder-like fault zone, rather than being focused on the mSAF, since the Pleistocene inception of the ladder structure. At the time scale of individual large earthquakes or creep events, however, slip might activate some portions of the ladder structure and not others, and slip might shift through the ladder structure in an unpredictable manner from one earthquake to the next.

CONCLUSIONS

We used geologic mapping and structural analyses to document the existence, activity, and regional significance of the previously unmapped and unknown Durmid ladder structure along the southern 30 km of the

SAFZ. A key newly documented element of this ladder structure is the right-lateral and reverse East Shoreline strand of the San Andreas fault along its southwest margin. The mSAF and ESF have a coordinated ladder-like geometry in Durmid Hill and bound many rotating blocks between them. The Durmid ladder structure is ~1–3 km wide and deforms a band of moderately consolidated sedimentary rocks northeast of the margin of the Salton Sea. It might involve another ~1–200 m of these units on the lake floor.

The Durmid ladder structure can be traced with confidence to the northeast corner of the Salton Sea from its termination at Bombay Beach, and, based on structures identified at the Mecca Hills and Desert Park to the northwest, it is proposed to continue north along the northeast edge of Coachella Valley to the Garnet Hill fault zone. Seismic data in the Mecca and Indio Hills indicate a northeast dip direction and suggest that the ESF is a key component of flower structures of the SAFZ along at least 100 km of the SAFZ.

The persistent shortening and transpression within the Durmid ladder structure, its northeast-up imprint on the landscape, and its relationship with much younger Holocene sediment of the Salton Sea indicate that there is a notable component of reverse slip across the right-lateral fault zone. The ESF probably merges with the mSAF at depth, and together they form a steeply northeast-dipping fault zone at depth, if the geometry imaged in seismic profiles in the southern Mecca Hills and Indio Hills is representative of the geometry in Durmid Hill (Fuis et al., 2017; Hernandez et al., 2015). A second branch of the ESF might cross the northern Coachella Valley and be linked to the poorly understood Palm Springs blind fault, but this connection is not as clear as the ESF–Garnet Hills correlation.

The southward widening of the Durmid ladder structure facilitates a smooth transition into the even wider BSZ in the southern Salton Sea. Thus, the San Andreas and Brawley fault zones together represent a curving fault zone of southward widening deformation that is ~1 km wide at the northern edge of the Salton Sea and >6 km wide along its southern edge (Fig. 1). In the vicinity of Bombay Beach, California, the fault zone changes southward from transpression and internal uplift into transtension and internal subsidence.

The great width of the ESF zone in Durmid Hill and the even larger width and spatial extent of the Durmid ladder structure imply that surface faulting hazards from a major earthquake rupture in this part of the SAFZ might be dispersed across a 40 km^2 area, if both master faults and the intervening cross faults are activated at once. If ladder-like strike-slip fault zones rupture in a piecemeal fashion, they will have an especially unpredictable surface-faulting hazard. The ladder model explains the geology, field relationships, and geophysical data sets at the southern tip of the SAFZ extremely well and shows that the southern 15 km section of the SAFZ is a strongly contractional variant of the transtensional BSZ farther south. Both ladder-like fault zones are likely to experience block rotation of cross faults, possibly at high rates. Prior pull-apart, sawtooth, transtensional, and cross-fault interpretations of this area need to be updated or reconsidered in light of these new results.

ACKNOWLEDGMENTS

This research was partly supported by the Southern California Earthquake Center (contribution 7224). Southern California Earthquake Center is funded by National Science Foundation Cooperative Agreement EAR-1033462 and U.S. Geological Survey Cooperative Agreement G12AC20038. The J.S. Williams fund contributed to field work conducted by Dan Markowski. We thank the staff of the Sonny Bono Wildlife Preserve for hospitality and accommodations during our first field season, and Robert Quinn for amazing hospitality and accommodations ever after. College of Science Dean Maura Hagan and the Department of Geology provided page charges. Egill Hauksson and Jennifer Anderson kindly shared relocated earthquakes produced by the September 2016 Bombay Beach swarm. We thank Michele Cooke for originally suggesting to Susanne that the ESF might be the Garnet Hill fault. Reviewer Sarah Titus, science editor Arlo Weil, and two anonymous reviewers provided many helpful suggestions, and we thank them.

REFERENCES CITED

Babcock, E.A., 1969, Structural Geology and Geophysics of the Durmid Area, Imperial Valley, California [Ph.D. dissertation], Riverside, California, University of California, 149 p.

Babcock, E.A., 1974, Geology of the northeast margin of the Salton Trough, Salton Sea, California: Geological Society of America Bulletin, v. 85, p. 321–332, https://doi.org/10.1130/0016-7606(1974)85<321:GOTNMO>2.0.CO;2.

Barak, S., Klemperer, S.L., and Lawrence, J.F., 2015, San Andreas fault dip, Peninsular Ranges mafic lower crust, and partial melt in the Salton Trough, southern California, from ambient-noise tomography: Geochemistry Geophysics Geosystems, v. 16, p. 3946–3972, https://doi.org/10.1002/2015GC005970.

Belgarde, B.E., 2007, Structural Characterization of Three Southeast Segments of the Clark Fault, Salton Trough, California [M.Sc. thesis]: Logan, Utah, Utah State University, 223 p., 3 plates.

Bilham, R., and Williams, P., 1985, Sawtooth segmentation and deformation processes on the southern San Andreas fault, California: Geophysical Research Letters, v. 12, p. 557–560, https://doi.org/10.1029/GL012i009p00557.

Brothers, D., Driscoll, N.W., Kent, G.M., Harding, A.J., Babcock, J.M., and Baskin, R.L., 2009, Tectonic evolution of the Salton Sea inferred from seismic reflection data: Nature Geoscience, v. 2, p. 581–584, https://doi.org/10.1038/ngeo590.

Brothers, D., Kilb, D., Luttrell, K., Driscoll, N., and Kent, G., 2011, Loading of the San Andreas fault by flood-induced rupture of faults beneath the Salton Sea: Nature Geoscience, v. 4, p. 486–492, https://doi.org/10.1038/ngeo1184.

Bryant, W.A., 2015, San Andreas, Hidden Spring, Skeleton Canyon, Mecca Hills, and Related Faults, Riverside and Imperial Counties, California: California Geological Survey Fault Evaluation Report FER-252, 29 p.

Bryant, W.A., and Hart, E.W., 2007, Fault Hazard Zones in California: California Geological Survey Special Publication 42, 38 p.

Bürgmann, R., 1991, Transpression along the southern San Andreas fault, Durmid Hill, California: Tectonics, v. 10, p. 1152–1163, https://doi.org/10.1029/91TC01443.

California Department of Water Resources (DWR), 1964, Coachella Valley Investigation: Bulletin 108, 145 p., 13 plates.

Carena, S., Suppe, J., and Kao, H., 2004, Lack of continuity of the San Andreas fault in southern California: Three-dimensional fault models and earthquake scenarios: Journal of Geophysical Research–Solid Earth, v. 109, no. B4, B04313, https://doi.org/10.1029/2003JB002643.

Clark, K.J., Nissen, E.K., Howarth, J.D., Hamling, I.J., Mountjoy, J.J., Ries, W.F., and Hreinsdóttir, S., 2017, Highly variable coastal deformation in the 2016 Mw7.8 Kaikōura earthquake reflects rupture complexity along a transpressional plate boundary: Earth and Planetary Science Letters, v. 474, p. 334–344, https://doi.org/10.1016/j.epsl.2017.06.048.

Clark, M.M., 1984, Map Showing Recently Active Breaks of the San Andreas Fault and Associated Faults Between Salton Sea and Whitewater River–Mission Creek, California: U.S. Geological Survey Miscellaneous Investigations Series Map I-1483, scale 1:24,000.

Dibblee, T.W., Jr., 1954, Geology of the Imperial Valley region, California, *in* Jahns, R.H., ed., Geology of Southern California: California Department of Natural Resources, Division of Mines Bulletin 170, p. 21–28.

Dibblee, T.W., Jr., 1984, Stratigraphy and tectonics of the San Felipe Hills, Borrego Badlands, Superstition Hills, and vicinity, *in* Rigby, C.A., ed., The Imperial Basin: Tectonics, Sedimentation, and Thermal Aspects: Field Trip Guidebook: Bakersfield, California, Pacific Section, Society of Economic Paleontologists and Mineralogists, Book 40, p. 31–44.

Dibblee, T.W., Jr., 1997, Geology of the southeastern San Andreas fault zone in the Coachella Valley, *in* Baldwin, J., Lewis, L., Payne, M., and Roquemore, G., eds., Southern San Andreas Fault: Whitewater to Bombay Beach, Salton Trough, California: Santa Ana, California, South Coast Geological Society, Annual Field Trip Guidebook 25, p. 35–56.

Dibblee, T.W., and Minch, J.A., 2008a, Geologic Map of the Cottonwood Spring and Canyon Spring Quadrangles, Riverside County, California: U.S. Geological Survey–Dibblee Geological Foundation Map DF-375, scale 1:62,500.

Dibblee, T.W., and Minch, J.A., 2008b, Geologic Map of the Palm Desert and Coachella 15 Minute Quadrangles, Riverside County, California: U.S. Geological Survey–Dibblee Geological Foundation Map DF-373, scale 1:62,500.

Dibblee, T.W., Jr., and Minch, J.A., 2008c, Geologic Map of the Durmid 15 Minute Quadrangle, Riverside and Imperial Counties, California: U.S. Geological Survey–Dibblee Geological Foundation Map DF-376, scale 1:62,500.

Dickinson, W.R., 1996, Kinematics of Transrotational Tectonism in the California Transverse Ranges and its Contribution to Cumulative Slip along the San Andreas Transform Fault System: Geological Society of America Special Paper 305, 46 p., https://doi.org/10.1130/0-8137-2305-1.1.

Dohrenwend, J.C., Gray, F., and Miller, R.J., 2001, Processed Landsat Thematic Mapper Satellite Imagery for Selected Areas Within the US-Mexico Borderlands (False Color Composite Image, Path 35 Row 38; Acquired on 24 June 1997, Band 7—Red; Band 4—Green; Band 2—Blue): U.S. Geological Survey Open-File Report 00–309.

Dorsey, R.J., and Langenheim, V.E., 2015, Crustal-scale tilting of the central Salton block, southern California: Geosphere, v. 11, no. 5, p. 1365–1383, https://doi.org/10.1130/GES01167.1.

Dorsey, R.J., Fluette, A., McDougall, K., Housen, B.A., Janecke, S.U., Axen, G.J., and Shirvell, C.R., 2007, Chronology of Miocene–Pliocene deposits at Split Mountain Gorge, southern California: A record of regional tectonics and Colorado River evolution: Geology, v. 35, p. 57–60, https://doi.org/10.1130/G23139A.1.

Dorsey, R.J., Housen, B.A., Janecke, S.U., Fanning, C.M., and Spears, A.L.F., 2011, Stratigraphic record of basin development within the San Andreas fault system: Late Cenozoic Fish Creek–Vallecito Basin, southern California: Geological Society of America Bulletin, v. 123, p. 771–793, https://doi.org/10.1130/B30168.1.

Fattaruso, L.A., Cooke, M.L., and Dorsey, R.J., 2014, Sensitivity of uplift patterns to the dip of the San Andreas fault in the Coachella Valley: Geosphere, v. 10, p. 1235–1246, https://doi.org/10.1130/GES01050.1.

Field, E.H., and 2014 Working Group on California Earthquake Probabilities, 2015, UCERF3: A New Earthquake Forecast for California's Complex Fault System: U.S. Geological Survey Fact Sheet 2015–3009, 6 p., http://dx.doi.org/10.3133/fs20153009.

Field, E.H., Arrowsmith, J.R., Biasi, G.P., Bird, P., Dawson, T.E., Felzer, K.R., Jackson, D.D., Johnson, K.M., Jordan, T.H., Madden, C., Michael, A.J., Milner, K.R., Page, M.T., Parsons, T., Powers, P.M., Shaw, B.E., Thatcher, W.R., Weldon, R.J., and Zeng, Y., 2014, Uniform California Earthquake Rupture Forecast, Version 3 (UCERF3)—The time-independent model: Bulletin of the Seismological Society of America, v. 104, p. 1122–1180, https://doi.org/10.1785/0120130164.

Fletcher, J.M., Teran, O.J., Rockwell, T.K., Oskin, M.E., Hudnut, K.W., Mueller, K.J., Spelz, R.M., Akciz, S.O., Masana, E., Faneros, G., and Fielding, E.J., 2014, Assembly of a large earthquake from a complex fault system: Surface rupture kinematics of the 4 April 2010 El Mayor–Cucapah (Mexico) Mw 7.2 earthquake: Geosphere, v. 10, p. 797–827, https://doi.org/10.1130/GES00933.1.

Fuis, G.S., Mooney, W.D., Healy, J.H., McMechan, G.A., and Lutter, W.J., 1982, Crustal Structure of the Imperial Valley Region, the Imperial Valley, California, Earthquake of October 15, 1979: U.S. Geological Survey Professional Paper 1254, p. 25–49.

Fuis, G.S., Mooney, W.D., Healy, J.H., McMechan, G.A., and Lutter, W.J., 1984, A seismic refraction survey of the Imperial Valley region, California: Journal of Geophysical Research–Solid Earth, v. 89, p. 1165–1189, https://doi.org/10.1029/JB089iB02p01165.

Fuis, G.S., Scheirer, D.S., Langenheim, V.E., and Kohler, M.D., 2012, A new perspective on the geometry of the San Andreas fault in southern California and its relationship to lithospheric structure: Bulletin of the Seismological Society of America, v. 102, p. 236–251, https://doi.org/10.1785/0120110041.

Fuis, G.S., Bauer, K., Goldman, M.R., Ryberg, T., Langenheim, V.E., Scheirer, D.S., Rymer, M.J., Stock, J.M., Hole, J.A., Catchings, R.D., and Graves, R.W., 2017, Subsurface geometry of the San Andreas fault in southern California: Results from the Salton Seismic Imaging Project (SSIP) and strong ground motion expectations: Bulletin of the Seismological Society of America, v. 107, no. 4, p. 1642–1662, https://doi.org/10.1785/0120160309.

Han, L., Hole, J.A., Stock, J.M., Fuis, G.S., Kell, A., Driscoll, N.W., Kent, G.M., Harding, A.J., Rymer, M.J., González-Fernández, A., and Lázaro-Mancilla, O., 2016a, Continental rupture and the creation of new crust in the Salton Trough rift, southern California and northern Mexico: Results from the Salton Seismic Imaging Project: Journal of Geophysical Research–Solid Earth, v. 121, no. 10, p. 7469–7489, https://doi.org/10.1002/2016JB013139.

Han, L., Hole, J.A., Stock, J.M., Fuis, G.S., Williams, C.F., Delph, J.R., Davenport, K.K., and Livers, A.J., 2016b, Seismic imaging of the metamorphism of young sediment into new crystalline crust in the actively rifting Imperial Valley, California: Geochemistry, Geophysics, Geosystems, v. 17, no. 11, p. 4566–4584.

Hauksson, E., Yang, W., and Shearer, P.M., 2012, Waveform relocated earthquake catalog for southern California (1981 to June 2011): Bulletin of the Seismological Society of America, v. 102, p. 2239–2244, https://doi.org/10.1785/0120120010.

Hauksson, E., Meier, M.A., Ross, Z.E., and Jones, L.M., 2017, Evolution of seismicity near the southernmost terminus of the San Andreas fault: Implications of recent earthquake clusters for earthquake risk in southern California: Geophysical Research Letters, v. 44, p. 1293–1301, https://doi.org/10.1002/2016GL072026.

Hernandez, A., Persaud, P., Bauer, K., Stock, J.M., Fuis, G., Hole, J., and Goldman, M., 2015, Constraints on shallow crustal structure across the San Andreas fault zone, Coachella Valley, southern California: Results from the Salton Seismic Imaging Project (SSIP): San Francisco, California, American Geophysical Union, Fall Meeting 2015, abstract T41A–2859.

Herzig, C.T., Mehegan, J.M., and Stelting, C.E., 1988, Lithostratigraphy of the State 2–14 borehole: Salton Sea Scientific Drilling Project: Journal of Geophysical Research–Solid Earth, v. 93, p. 12,969–12,980, https://doi.org/10.1029/JB093iB11p12969.

Hope, R.A., 1969, Map Showing Recently Active Breaks Along the San Andreas and Related Faults Between Cajon Pass and Salton Sea, California: U.S. Geological Survey Open-File Report OF-69–130, scale 1:24,000.

Hudnut, K.W., Seeber, L., and Pacheco, J., 1989a, Cross-fault triggering in the November 1987 Superstition Hills earthquake sequence, southern California: Geophysical Research Letters, v. 16, p. 199–202, https://doi.org/10.1029/GL016i002p00199.

Hudnut, K., Seeber, L., Rockwell, T., Goodmacher, J., Klinger, R., Lindvall, S., and McElwain, R., 1989b, Surface ruptures on cross-faults in the 24 November 1987 Superstition Hills, California, earthquake sequence: Bulletin of the Seismological Society of America, v. 79, p. 282–296.

Izett, G.A., Obradovich, J.D., and Mehnert, H.H., 1988, The Bishop Ash Bed (Middle Pleistocene) and Some Older (Pliocene and Pleistocene) Chemically Similar Ash Beds in California, Nevada, and Utah: U.S. Geological Survey Bulletin 1675, 37 p.

Janecke, S.U., 2013, Final Report for 2012 Southern California Earthquake Center Grant, Testing a Step-Over Model of the Southern San Andreas Fault at Durmid Hill: Los Angeles, California, Southern California Earthquake Center, 8 p., http://sceccore2.usc.edu/proposalfiles/2012reports/Janecke_12137_report.pdf.

Janecke, S.U., and Markowski, D., 2013, New structures from the southern tip of the San Andreas fault zone near Durmid Hill, 2013 Southern California Earthquake Center Annual Meeting Proceedings: Los Angeles, California, Southern California Earthquake Center, p. 199.

Janecke, S.U., and Markowski, D., 2015a, Character and implications of a newly identified creeping strand of the San Andreas fault northeast of Salton Sea, southern California, *in* 2015 Southern California Earthquake Center Annual Meeting Proceedings: Los Angeles, California, Southern California Earthquake Center, poster number 72.

Janecke, S.U., and Markowski, D., 2015b, Character and implications of a newly identified creeping strand of the San Andreas fault northeast of Salton Sea, southern California: San Francisco, California, American Geophysical Union, 2015 Fall Meeting, abstract T41A–2870.

Janecke, S.U. and Markowski, D.K., 2016 (revised from 2013 original), Revised SCEC Final report on the East Shoreline strand of the San Andreas fault: SCEC database http://scecinfo.usc.edu/core/cis/list_reports.php, 170 p.

Janecke, S.U., Dorsey, R.J., and Belgarde, B., 2010a, Age and structure of the San Jacinto and San Felipe fault zones and their lifetime slip rates, *in* Clifton, H.E., and Ingersoll, R.V., eds., Geologic Excursions in California and Nevada: Tectonics, Stratigraphy and Hydrogeology: Bakersfield, California, Pacific Section, Society for Sedimentary Geology, Book 108, p. 233–271.

Janecke, S.U., Dorsey, R.J., Forand, D., Steely, A.N., Kirby, S.M., Lutz, A.T., Housen, B.A., Belgarde, B., Langenheim, V.E., and Rittenour, T.M., 2010b, High Geologic Slip Rates Since Early Pleistocene Initiation of the San Jacinto and San Felipe Fault Zones in the San Andreas Fault System: Southern California, USA: Geological Society of America Special Paper 475, 48 p., https://doi.org/10.1130/2010.2475.

Janecke, S.U., Markowski, D., Bilham, R., Evans, J.P., Bunds, M., Wells, J., Andreini, J., and Quinn, R., 2016, The East Shoreline strand of the San Andreas fault and its implications for the next Big One in southern California, 2016 Southern California Earthquake Center Annual Meeting Proceedings: Los Angeles, California, Southern California Earthquake Center.

Jennings, C.W., 1967, Geologic Map of California: Salton Sea Sheet: Sacramento, California, California Division of Mines and Geology, scale 1:250,000.

Jennings, C.W., 1994, Fault Activity Map of California and Adjacent Areas with Location and Ages of Recent Volcanic Eruptions: California Division of Mines and Geology California Geologic Data Map Series 6, scale 1:750,000.

Johnson, C.E., and Hadley, D.M., 1976, Tectonic implications of the Brawley earthquake swarm, Imperial Valley, California, January 1975: Bulletin of the Seismological Society of America, v. 66, p. 1133–1144.

Jones, L.M., et al., 2008, The ShakeOut Scenario: U.S. Geological Survey Open-File Report 2008-1150, v. 1.0, 312 p.

Jordan, T., 2016, Locked, Loaded and Ready to Roll: http://www.latimes.com/local/lanow/la-me-ln-san-andreas-fault-earthquake-20160504-story.html (accessed 23 June 2016).

Kell, A.M., 2014, The Application of Active-Source Seismic Imaging Techniques to Transtensional Problems: The Walker Lane and Salton Trough [Ph.D. thesis]: Reno, Nevada, University of Nevada, 138 p.

Kirby, S.M., Janecke, S.U., Dorsey, R.J., Housen, B.A., McDougall, K., Langenheim, V., and Steely, A., 2007, Pleistocene Brawley and Ocotillo formations: Evidence for initial strike-slip deformation along the San Felipe and San Jacinto fault zones, California: Geology, v. 115, p. 43–62, https://doi.org/10.1086/509248.

Kroll, K.A., Cochran, E.S., Richards-Dinger, K.B., and Sumy, D.F., 2013, Aftershocks of the 2010 Mw 7.2 El Mayor–Cucapah earthquake reveal complex faulting in the Yuha Desert, California: Journal of Geophysical Research–Solid Earth, v. 118, p. 6146–6164, https://doi.org/10.1002/2013JB010529.

Langenheim, V.E., and Powell, R.E., 2009, Basin geometry and cumulative offsets in the Eastern Transverse Ranges, southern California: Implications for transrotational deformation along the San Andreas fault system: Geosphere, v. 5, p. 1–22, https://doi.org/10.1130/GES00177.1.

Langenheim, V.E., Athens, N., Scheirer, D., Fuis, G., Rymer, M., and Goldman, M., 2014, Width and dip of the southern San Andreas fault at Salt Creek from modeling of geophysical data, *in* Reynolds, R.E., ed., Not a Drop Left to Drink: 2014 Desert Symposium, April 2014: Fullerton, California, California State University, Desert Studies Center, p. 83–93.

Lin, G., 2013, Three-dimensional seismic velocity structure and precise earthquake relocations in the Salton Trough, southern California: Bulletin of the Seismological Society of America, v. 103, p. 2694–2708, https://doi.org/10.1785/0120120286.

Lin, G., Shearer, P.M., and Hauksson, E., 2007, Applying a three-dimensional velocity model, waveform cross correlation, and cluster analysis to locate southern California seismicity from 1981 to 2005: Journal of Geophysical Research. Solid Earth, v. 112, B12309, https://doi.org/10.1029/2007JB004986.

Lindsey, E.O., and Fialko, Y., 2013, Geodetic slip rates in the southern San Andreas fault system: Effects of elastic heterogeneity and fault geometry: Journal of Geophysical Research–Solid Earth, v. 118, p. 689–697, https://doi.org/10.1029/2012JB009358.

Lindsey, E.O., Fialko, Y., Bock, Y., Sandwell, D.T., and Bilham, R., 2014, Localized and distributed creep along the southern San Andreas fault: Journal of Geophysical Research, v. 119, p. 7909–7922, https://doi.org/10.1002/2014jb011275.

Lindvall, S.C. and Lindvall, Richter, and Associates, 1989, Investigation of the Surface Fault Rupture Hazard in the Special Study Zones of Bombay Beach, California: California Geological Survey Open-File Report 081889, LRA Report No. 158-01, 33 p., 5 plates, 2 p. transmittal letter.

Lutz, A.T., Dorsey, R.J., Housen, B.A., and Janecke, S.U., 2006, Stratigraphic record of Pleistocene faulting and basin evolution in the Borrego Badlands, San Jacinto fault zone, southern California: Geological Society of America Bulletin, v. 118, p. 1377–1397, https://doi.org/10.1130/B25946.1.

Lynch, D.K., and Hudnut, K.W., 2008, The Wister mud pot lineament: Southeastward extension or abandoned strand of the San Andreas fault?: Bulletin of the Seismological Society of America, v. 98, p. 1720–1729, https://doi.org/10.1785/0120070252.

Magistrale, H., 2002, The relation of the southern San Jacinto fault zone to the Imperial and Cerro Prieto faults, *in* Barth, A., ed., Contributions to Crustal Evolution of the Southwestern United States: Geological Society of America Special Paper 365, p. 271–278, https://doi.org/10.1130/0-8137-2365-5.271.

Markowski, D., 2016, Confirmation of a New Geometric and Kinematic Model of the San Andreas Fault at its Southern Tip, Durmid Hill, Southern California [M.S. thesis]: Logan, Utah, Utah State University, 133 p., 2 plates, http://digitalcommons.usu.edu/etd/4987/.

McNabb, J.C., Dorsey, R.J., Housen, B.A., Dimitroff, C.W., and Messé, G.T., 2017, Stratigraphic record of Pliocene–Pleistocene basin evolution and deformation within the southern San Andreas fault zone, Mecca Hills, California: Tectonophysics, v. 719, p. 66–85, https://doi.org/10.1016/j.tecto.2017.03.021.

Meltzner, A.J., Rockwell, T.K., Tsang, R.Y., and Figueiredo, P.M., 2016, Slip variability and temporal clustering along the Imperial fault at Mesquite Basin, Imperial Valley, California, and possible through-going rupture to the San Andreas fault, 2016 Southern California

Earthquake Center Annual Meeting Proceedings: Los Angeles, California, Southern California Earthquake Center, p. 210.
Milliner, C.W., Dolan, J.F., Hollingsworth, J., Leprince, S., Ayoub, F., and Sammis, C.G., 2015, Quantifying near-field and off-fault deformation patterns of the 1992 Mw 7.3 Landers earthquake: Geochemistry Geophysics Geosystems, v. 16, p. 1577–1598, https://doi.org/10.1002/2014GC005693.
Nicholson, C., 1996, Seismic behavior of the San Andreas fault in the Northern Coachella Valley, California: Comparison of the 1948 and 1986 earthquake sequences: Bulletin of the Seismological Society of America, v. 86, p. 1331–1349.
Nicholson, C., Seeber, L., Williams, P., and Sykes, L.R., 1986, Seismic evidence for conjugate slip and block rotation within the San Andreas fault system, southern California: Tectonics, v. 5, p. 629–648, https://doi.org/10.1029/TC005i004p00629.
Olsen, K.B., Archuleta, R.J., and Matarese, J.R., 1995, Three-dimensional simulation of a magnitude 7.75 earthquake on the San Andreas fault: Science, v. 270, p. 1628, https://doi.org/10.1126/science.270.5242.1628.
Olsen, K.B., Day, S.M., Minster, J.B., Cui, Y., Chourasia, A., Faerman, M., Moore, R., Maechling, P., and Jordan, T., 2006, Strong shaking in Los Angeles expected from southern San Andreas earthquake: Geophysical Research Letters, v. 33, L07305, https://doi.org/10.1029/2005GL025472.
Olsen, K.B., Day, S.M., Dalguer, L.A., Mayhew, J., Cui, Y., Zhu, J., Cruz-Atienza, V.M., Roten, D., Maechling, P., Jordan, T.H., and Okaya, D., 2009, ShakeOut-D: Ground motion estimates using an ensemble of large earthquakes on the southern San Andreas fault with spontaneous rupture propagation: Geophysical Research Letters, v. 36, L04303, https://doi.org/10.1029/2008GL036832.
Open Topography, 2005, B4 Project–Southern San Andreas and San Jacinto Faults: http://opentopo.sdsc.edu/datasetMetadata?otCollectionID=OT.032006.32611.1 (accessed many times).
Persaud, P., Ma, Y., Stock, J.M., Hole, J.A., Fuis, G.S., and Han, L., 2016, Fault zone characteristics and basin complexity in the southern Salton Trough, California: Geology, v. 44, p. 747–750, https://doi.org/10.1130/G38033.1.
Petra Geoscience, Inc., 2009, Geotechnical Investigation Report for Posse Park Property, Project Number 322-08: City of Indio, Riverside County, California, Indio Water Authority.
Philibosian B., Fumal T., and Weldon R., 2011, San Andreas fault earthquake chronology and Lake Cahuilla history at Coachella, California: Seismological Society of America Bulletin, v. 101, p. 13–38, https://doi.org/10.1785/0120100050.
Redlands Institute, 1999, Salton Sea 1 Meter Bathymetric Contour and Metadata: http://www.spatial.redlands.edu/salton/data/gisdata.aspx and http://www.spatial.redlands.edu/salton/Downloads/Shapefiles/Metadata/ss_bathymetry_1m_metadata.htm#7 (accessed 17 June 2016).
Robbins, S., and Reyes, P., 2012, Coachella Valley Water Management Plan 2010 Update: Coachella Valley Water District, http://www.cvwd.org/DocumentCenter/Home/View/2130 (accessed 21 December 2017).
Rockwell, T., 2016, Open intervals, clusters and supercycles: 1100 years of Moment release in the southern San Andreas Fault system: Are we ready for the century of earthquakes?: Southern California Earthquake Center, https://files.scec.org/s3fs-public/publication_6367.pdf (accessed 26 April 2018).
Rockwell, T.K., Meltzner, A., and Tsang, R., 2011, A Long Record of Earthquakes with Timing and Displacements for the Imperial Fault: A Test of Earthquake Recurrence Models: U.S. Geological Survey Final Technical Report for USGS Grant No. G10AP00003, 70 p.
Rogers, T.H., 1965, Geologic Map of California: Santa Ana Sheet: Sacramento, California, California Division of Mines and Geology, scale 1:250,000.
Ross, Z.E., Hauksson, E., and Ben-Zion, Y., 2017, Abundant off-fault seismicity and orthogonal structures in the San Jacinto fault zone: Science Advances, v. 3, no. 3, https://doi.org/10.1126/sciadv.1601946.
Roten, D., Olsen, K.B., Day, S.M., Cui, Y., and Fäh, D., 2014, Expected seismic shaking in Los Angeles reduced by San Andreas fault zone plasticity: Geophysical Research Letters, v. 41, p. 2769–2777, https://doi.org/10.1002/2014GL059411.
Sahakian, V.J., 2015 Architecture and Segmentation of Strike-Slip Faults in Southern California [Ph.D. dissertation]: San Diego, California, University of California, 116 p.
Sahakian, V.J., Holmes, J.J., Kell, A.M., Harding, A.J., Driscoll, N.W., and Kent, G., 2013, New constraints on the geometry and evolution of the southern San Andreas fault and Salton pull-apart basin: San Francisco, California, American Geophysical Union, Fall Meeting 2013, abstract T11D–2481.
Sahakian, V.J., Kell, A.M., Holmes, J.J., Harding, A.J., Driscoll, N.W., and Kent, G., 2014, Geophysical evidence for a southwestward dipping southern San Andreas fault, *in* 2014 Southern California Earthquake Center Annual Meeting: Los Angeles, California, Southern California Earthquake Center, poster 206.
Sahakian, V., Kell, A., Harding, A., Driscoll, N., and Kent, G., 2016, Geophysical evidence for a San Andreas subparallel transtensional fault along the northeastern shore of the Salton Sea: Bulletin of the Seismological Society of America, v. 106, p. 1963–1978, https://doi.org/10.1785/0120150350.
Salton Sea LiDAR Collection, 2010, Salton Sea LiDAR Collection: http://opentopo.sdsc.edu/datasetMetadata?otCollectionID=OT.032012.26911.2 (accessed many times).
Sarna-Wojcicki, A.M., Pringle, M.S., and Wijbrans, J., 2000, New Ar/Ar age of the Bishop Tuff from multiple sites and sediment rate calibration for the Matuyama-Brunhes boundary: Journal of Geophysical Research, v. 105, p. 21,431–21,443.
Schmitt, A.K., Martín, A., Stockli, D.F., Farley, K.A., and Lovera, O.M., 2013, (U-Th)/He zircon and archaeological ages for a late prehistoric eruption in the Salton Trough (California, USA): Geology, v. 41, p. 7–10, https://doi.org/10.1130/G33634.1.
Sharp, R.V., 1967, San Jacinto fault zone in the Peninsular Ranges of southern California: Geological Society of America Bulletin, v. 78, p. 705–730, https://doi.org/10.1130/0016-7606(1967)78[705:SJFZIT]2.0.CO;2.
Sharp, R.V., Lienkaemper, J.J., Bonilla, M.G., Burke, D.B., Cox, B.F., Herd, D.G., Miller, D.M., Morton, D.M., Ponti, D.J., Rymer, M.J., Tinsley, J.C., and Yount, J.C., 1982, Surface faulting in the central Imperial Valley, *in* The Imperial Valley, California, Earthquake of October 15, 1979: U.S. Geological Survey Professional Paper 1254, p. 119–144.
Shearer, P., Hauksson, E., and Lin, G., 2005, Southern California hypocenter relocation with waveform cross-correlation, part 2: Results using source-specific station terms and cluster analysis: Bulletin of the Seismological Society of America, v. 95, p. 904–915, https://doi.org/10.1785/0120040168.
Sieh, K.E., and Williams, P.L., 1990, Behavior of the southernmost San Andreas fault during the past 300 years: Journal of Geophysical Research, v. 95, p. 6629–6645, https://doi.org/10.1029/JB095iB05p06629.
Steely, A.N., 2006, The Evolution from Late Miocene West Salton Detachment Faulting to Cross-Cutting Pleistocene Oblique Strike-Slip Faults in the SW Salton Trough, Southern California [M.Sc. thesis]: Logan, Utah, Utah State University, 242 p., 3 plates.
Steely, A.N., Janecke, S.U., Axen, G.J., and Dorsey, R.J., 2009, Pleistocene reorganization of the southern San Andreas fault system: Initiation and structures of the San Felipe fault zone: Geological Society of America Bulletin, v. 121, p. 663–687, https://doi.org/10.1130/B26239.1.
Strauss, B., 2011, Bishop Ash AMS fabric adjacent to the southernmost segment of the San Andreas fault, Durmid Hill, Salton Trough, California: Geological Society of America Abstracts with Programs, v. 43, no. 5, p. 607.
Sylvester, A.G., 1988, Strike-slip faults: Geological Society of America Bulletin, v. 100, p. 1666–1703, https://doi.org/10.1130/0016-7606(1988)100<1666:SSF>2.3.CO;2.
Sylvester, A.G., and Smith, R.R., 1976, Tectonic transpression and basement-controlled deformation in San Andreas fault zone, Salton Trough, California: American Association of Petroleum Geologists Bulletin, v. 60, p. 2081–2102.
Sylvester, A.G., Bilham, R., Jackson, M., and Barrientos, S., 1993, Aseismic growth of Durmid Hill, southeasternmost San Andreas fault, California: Journal of Geophysical Research–Solid Earth, v. 98, p. 14,233–14,243, https://doi.org/10.1029/93JB01028.
Thornock, S.J., 2013, Southward Continuation of the San Jacinto Fault Zone through and beneath the Extra and Elmore Ranch Left-Lateral Fault Arrays, Southern California [M.S. thesis]: Logan, Utah, Utah State University, 223 p., 1 plate, http://digitalcommons.usu.edu/etd/1978.
Tong, X., Sandwell, D.T., and Smith-Konter, B., 2013, High-resolution interseismic velocity data along the San Andreas fault from GPS and InSAR: Journal of Geophysical Research–Solid Earth, v. 118, p. 369–389, https://doi.org/10.1029/2012JB009442.
Tong, X., Smith-Konter, B., and Sandwell, D.T., 2014, Is there a discrepancy between geological and geodetic slip rates along the San Andreas fault system?: Journal of Geophysical Research–Solid Earth, v. 119, p. 2518–2538, https://doi.org/10.1002/2013JB010765.
Winker, C.D., 1987, Neogene Stratigraphy of the Fish Creek–Vallecito Section, Southern California: Implications for Early History of the Northern Gulf of California and Colorado delta [Ph.D. thesis]: Tucson, Arizona, University of Arizona, 494 p.
Yang, W., and Hauksson, E., 2013, The tectonic crustal stress field and style of faulting along the Pacific North America plate boundary in southern California: Geophysical Journal International, v. 194, no. 1, p. 100–117, https://doi.org/10.1093/gji/ggt113.
Zeeden, C., Rivera, T.A., and Storey, M., 2014, An astronomical age for the Bishop Tuff and concordance with radioisotopic dates: Geophysical Research Letters, v. 41, p. 3478–3484, https://doi.org/10.1002/2014GL059899.

MANUSCRIPT RECEIVED 11 NOVEMBER 2016
REVISED MANUSCRIPT RECEIVED 31 MARCH 2018
MANUSCRIPT ACCEPTED 15 MAY 2018